sustainability

MDPI

Article

Load Frequency Control and Automatic Voltage Regulation in a Multi-Area Interconnected Power System Using Nature-Inspired Computation-Based Control Methodology

Tayyab Ali [1], Suheel Abdullah Malik [1], Ibrahim A. Hameed [2,*], Amil Daraz [3], Hana Mujlid [4] and Ahmad Taher Azar [5,6,7,*]

[1] Department of Electrical Engineering, FET, International Islamic University, Islamabad 44000, Pakistan
[2] Department of ICT and Natural Sciences, Norwegian University of Science and Technology, Larsgårdsve-gen, 2, 6009 Ålesund, Norway
[3] School of Information Science and Engineering, Ningbotech University, Ningbo 315100, China
[4] Department of Computer Engineering, Taif University, Taif 21944, Saudi Arabia
[5] College of Computer and Information Sciences, Prince Sultan University, Riyadh 11586, Saudi Arabia
[6] Automated Systems and Soft Computing Lab (ASSCL), Prince Sultan University, Riyadh 12435, Saudi Arabia
[7] Faculty of Computers and Artificial Intelligence, Benha University, Benha 13518, Egypt
* Correspondence: ibib@ntnu.no (I.A.H.); aazar@psu.edu.sa or ahmad.azar@fci.bu.edu.eg or ahmad_t_azar@ieee.org (A.T.A.)

Abstract: The stability control of nominal frequency and terminal voltage in an interconnected power system (IPS) is always a challenging task for researchers. The load variation or any disturbance affects the active and reactive power demands, which badly influence the normal working of IPS. In order to maintain frequency and terminal voltage at rated values, controllers are installed at generating stations to keep these parameters within the prescribed limits by varying the active and reactive power demands. This is accomplished by load frequency control (LFC) and automatic voltage regulator (AVR) loops, which are coupled to each other. Due to the complexity of the combined AVR-LFC model, the simultaneous control of frequency and terminal voltage in an IPS requires an intelligent control strategy. The performance of IPS solely depends upon the working of the controllers. This work presents the exploration of control methodology based on a proportional integral–proportional derivative (PI-PD) controller with combined LFC-AVR in a multi-area IPS. The PI-PD controller was tuned with recently developed nature-inspired computation algorithms including the Archimedes optimization algorithm (AOA), learner performance-based behavior optimization (LPBO), and modified particle swarm optimization (MPSO). In the earlier part of this work, the proposed methodology was applied to a two-area IPS, and the output responses of LPBO-PI-PD, AOA-PI-PD, and MPSO-PI-PD control schemes were compared with an existing nonlinear threshold-accepting algorithm-based PID (NLTA-PID) controller. After achieving satisfactory results in the two-area IPS, the proposed scheme was examined in a three-area IPS with combined AVR and LFC. Finally, the reliability and efficacy of the proposed methodology was investigated on a three-area IPS with LFC-AVR with variations in the system parameters over a range of Â ± 50%. The simulation results and a comprehensive comparison between the controllers clearly demonstrates that the proposed control schemes including LPBO-PI-PD, AOA-PI-PD, and MPSO-PI-PD are very reliable, and they can effectively stabilize the frequency and terminal voltage in a multi-area IPS with combined LFC and AVR.

Keywords: PI-PD controller; load frequency control; automatic voltage regulator; nature-inspired optimization; multi-area interconnected power system

Citation: Ali, T.; Malik, S.A.; Hameed, I.A.; Daraz, A.; Mujlid, H.; Azar, A.T. Load Frequency Control and Automatic Voltage Regulation in a Multi-Area Interconnected Power System Using Nature-Inspired Computation-Based Control Methodology. *Sustainability* **2022**, *14*, 12162. https://doi.org/10.3390/su141912162

Academic Editors: Herodotos Herodotou, Sheraz Aslam and Nouman Ashraf

Received: 19 August 2022
Accepted: 20 September 2022
Published: 26 September 2022

Publisher's Note: MDPI stays neutral with regard to jurisdictional claims in published maps and institutional affiliations.

1. Introduction

Research efforts and specializations in power systems are increasing day by day to acquire reliable power with nominal voltage and frequency. In a power system, the main

goal is to provide nominal voltage and frequency to all consumers without any interruption. The simultaneous control of load frequency and terminal voltage in an interconnected electrical power system is the fundamental area of research for all practicing engineers. The mutilation of frequency or voltage can spoil the performance and life expectancy of equipment associated with IPS [1]. The active and reactive powers can change with load demands in IPS. The active power can be adjusted by a speed governor in an LFC loop, whereas reactive power can be controlled by an exciter in an AVR loop. In order to fulfill the active power demand, a turbine input is continuously regulated in LFC, or else the changing frequency will vary the machine's speed. In AVR, terminal voltage remains within the prescribed limit if the excitation of generators is regulated properly to match the reactive power demand. A lot of literature is available on individual AVR or LFC systems; however, relatively less research work has been carried out on combined LFC-AVR due to its complex design. The PID controller was extensively used in multi-area IPS due to its simple design and easier installation. For instance, the artificial electric field algorithm-based hybridized approach to tune the fuzzy PID controller was suggested for combined LFC and AVR with the incorporation of different energy storage devices [1]. A particle swarm-optimized Ziegler–Nicholas (PSO-ZN)-based PID controller was examined for AVR-LFC control in PV integration and a conventional power system [2]. PI and PID with filter (PIDF) controllers based on the sine cosine algorithm were also inquired for a two-area, two-source IPS. The redox flow batteries were assimilated for further improvements in the system dynamics [3]. The doctor and patient optimization (DPO)-based accelerating PID controller (PIDA) was proposed for the LFC-AVR problem in a multi-area IPS with renewable energy sources [4]. The PID controller was employed for collective AVR-LFC in a two-area IPS. A nonlinear threshold-accepting algorithm was explored to find the optimum parameters of the PID controller [5]. PI and I controllers for AVR and an LFC loop were also investigated for a single-area IPS [6]. In [7], due to the inclusion of deregulated environments in IPS, a fuzzy logic controller (FLC) was recommended for a two-area LFC-AVR problem. A fractional order controller ($PID^{\mu}F$) based on the lightning search algorithm (LSA) was also proposed for LFC-AVR with wind and a reheat thermal plant as the generating companies (GENCOs) of area-1,and with diesel and a nonlinear reheat thermal plant as the GENCOs of area-2 under deregulated environments [8].The PID controller was optimized with the hybridization of the artificial electric field algorithm and differential evolution for a two-area IPS with a joint LFC-AVR [9,10]. In [11], PID with the firefly algorithm was employed for a two-area IPS with AVR-LFC. The moth flame optimization (MFO)-based fractional order PID controller was proposed for both LFC and AVR loops [12]. For a single-area synchronous generator, the combined LFC-AVR was explored using a hardware environment [13]. In [14,15], the authors inspected the firefly algorithm, particle swarm optimization, and the genetic algorithm-based PID controller for AVR-LFC loops. The novel state-observer (SO)-based integral double-derivative controller based on magneto-tactic-bacteria optimization (MBO) was presented for voltage–frequency control in a hybrid IPS [16]. The model predictive controller (MPC) was also used to improve AVR-LFC responses [17]. In [18], the heuristic computation-based two degrees of freedom state-feedback PI controller was exploited for the AVR loop in synchronous generators. A combination of the bacterial foraging optimization algorithm and particle swarm optimization was utilized to tune the PI controller for the AVR system with a static synchronous compensator [19]. In [20], a sliding mode controller with the addition of a gene ralized extended state observer was successfully explored to optimize the LFC loop in a multi-area IPS. The PID controller tuned with the many optimizing liaisons (MOL) algorithm was applied to a two-area IPS with non-reheat thermal sources in the presence of GDB [21]. Moreover, a comprehensive research work was presented for individual LFC loops as presented in [22–37]. A brief literature summary of AVR-LFC is provided in Table 1. It can be seen that much less attention has been given to the combined LFC-AVR problem in multi-area IPS due to its complex structure. The literature survey also depicts that modified forms of the PID controller were explored very rarely for combined AVR-LFC. Different

modified forms such as PI, PIDF, PID$^{\mu}$F, and FO-IDF have been explored due to their excellent time response characteristics with fast convergence, but the PI-PD controller has not been employed for combined LFC-AVR multi-area IPS. Due to its modified structure having a control branch in the feedback path, complex systems can be well optimized with PI-PD as compared to classical control schemes such PI and PID, etc. To obtain optimal controller parameters, an intelligent tuning algorithm is needed, which can optimize the controller with minimum error/fitness. In the past, nature-inspired optimization algorithms have received a lot of attention from researchers because of their strengths and abilities to tackle a variety of complex optimization issues in engineering. These strategies have also been used successfully to obtain optimal controller parameters. The classical nature-inspired computing techniques have shown very satisfactory performances for both individual and combined LFC-AVR. Moreover, researchers have also presented some novel nature-computing algorithms such as dandelion optimizer [38], modified particle swarm optimization (MPSO), bald eagle search (BES) [39], the transient search algorithm (TSO) [40], learner performance-based behavior optimization (LPBO) [41], the Archimedes optimization algorithm (AOA) [42], etc. These recently introduced techniques such as MPSO, LPBO, and AOA have not been considered for the optimal tuning of the PI-PD control scheme. It will be worth choosing these nature-inspired techniques for the optimization of multi-area IPS with combined LFC-AVR. Keeping in mind the existing research gap, the nature-inspired computation-based PI-PD control scheme is proposed in this research for multi-area IPS with combined AVR-LFC. The main contributions of this work are:

1. The modeling of combined AVR-LFC for two-area and three-area IPS;
2. The modeling of the PI-PD control scheme and its optimization using the Archimedes optimization algorithm (AOA), learner performance-based behavior optimization (LPBO), and modified particle swarm optimization (MPSO);
3. The formulation of fitness functions for the optimization of proposed controller;
4. Further, a comprehensive performance comparison is carried out between LPBO-PI-PD, AOA-PI-PD, and MPSO-PI-PD in two-area IPS. Moreover, the efficacy of the proposed control schemes has been tested in a three-area IPS with a combined LFC-AVR problem;
5. The reliability of the proposed control methodology has been illustrated by altering the system parameters of three-area IPS over a range of Â ± 50%.

Table 1. Literature on ALR-LFC.

Reference	Year	Research Area	Controller	Tuning Schemes	Area/System	Nonlinearities	Additional Incorporation
[2]	2021	AVR-LFC	PID	PSO-ZN	Two Area	-	-
[3]	2020	AVR-LFC	PI, PIDF	CSA	Two Area	-	RFBs, UPFC
[4]	2022	AVR-LFC	PIDA	DPO	Two Area		-
[5]	2019	AVR-LFC	PID	NLTA	Single Area	-	-
[6]	2014	AVR-LFC	PI	Not given	Single Area	-	Damper Winding
[7]	2019	AVR-LFC	PID, FLC	Fuzzy Logic	Two Area	-	DC Link, Deregulated Environment
[8]	2018	AVR-LFC	PIDF, PID$^{\mu}$F	LSA	Two Area	GDB, GRC	SMES, IPFC, Deregulated Environment
[9]	2020	AVR-LFC	PID	DE-AEFA	Two Area	GRC	IPFC and RFBs
[10]	2020	AVR-LFC	PID	DE-AEFA	Two Area	GRC	HVDC link with the existing AC tie-line
[11]	2019	AVR-LFC	PID	FO	Two Area	-	-
[12]	2019	AVR-LFC	FO-PID	MFO	Two Area	GDB, BD	-
[13]	2020	AVR-LFC	PI	HIL Strategy	Single Area	-	-
[14]	2019	AVR-LFC	PID	FA, GA, PSO	Single Area	-	-

Table 1. *Cont.*

Reference	Year	Research Area	Controller	Tuning Schemes	Area/System	Nonlinearities	Additional Incorporation
[15]	2015	AVR-LFC	PID	PSO	Two Area	-	-
[16]	2018	AVR-LFC	SO-IDD	MBO	Two Area	GRC, GDB	-
[17]	2020	AVR-LFC	MPC	MPC	Two Area	-	-
[18]	2020	AVR	2DOF state-feedback PI control	VSA, WOA, SCA GWO, SSA, WCA	AVR for Synchronous Generator	-	-
[19]	2021	AVR	PI	Hybrid BFOA-PSO	Standalone Wind–Diesel Power System	-	STATCOM
[20]	2019	LFC	Observer-based nonlinear sliding mode control	LMI	Two Area	GRC, GDB	-
[21]	2021	LFC	PID	MOL	Two Area	GDB	-
Proposed Work	2022	AVR-LFC	PI-PD	AOA, LPBO, MPSO	Two Area, Three Area	-	-

Table 2 demonstrates the nomenclature used in this study. This research paper is organized in following way: The power system model is described in Section 2. The proposed control methodology is presented in Section 3. Section 4 contains a description and flow charts of nature-inspired computation algorithms including LPBO, AOA, and MPSO. The implementation and results of the proposed techniques are summarized in Section 5. Lastly, conclusions and future guidelines are given in Section 6.

Table 2. Nomenclature.

Acronym	Definition	Acronym	Definition
AOA	Archimedes optimization algorithm	IPS	Interconnected power system
NLTA	Nonlinear threshold-accepting algorithm	LPBO	Learner performance-based behavior optimization
AVR	Automatic voltage regulator	ΔP_{tie}	Tie-line power deviation
PI-PD	Proportional integral–proportional derivative	V_t	Terminal voltage
MPSO	Modified particle swarm optimization	LFC	Load frequency control
R_i	Speed regulation	Δf	Frequency deviation
K_G	Governor gain	B	Area bias factor
T_G	Time constant of governor	ΔP_D	Load deviation
K_a	Amplifier gain	K_t	Turbine gain
T_a	Time constant of amplifier	T_t	Time constant of turbine
K_g	Generator gain	K_e	Exciter gain
T_g	Time constant of generator	T_e	Time constant of exciter
K_p	Power system gain	ΔX_G	Valve position of governor
T_p	Time constant of power system	ΔP_G	Deviation in the output of generator
T_{12}, T_{21}	Tie-line synchronizing time constants	K_i	Coupling coefficient of AVR-LFC loops

2. Power System Model

The multi-area IPS model under study is shown in Figure 1. The terminal voltage was maintained at nominal value by stabilizing the generator fields, while the load frequency was regulated by controlling real power. Figure 1a represents the AVR-LFC model of a power system for a single area, where *i* and *j* represent area-1 and area-2, respectively [5].

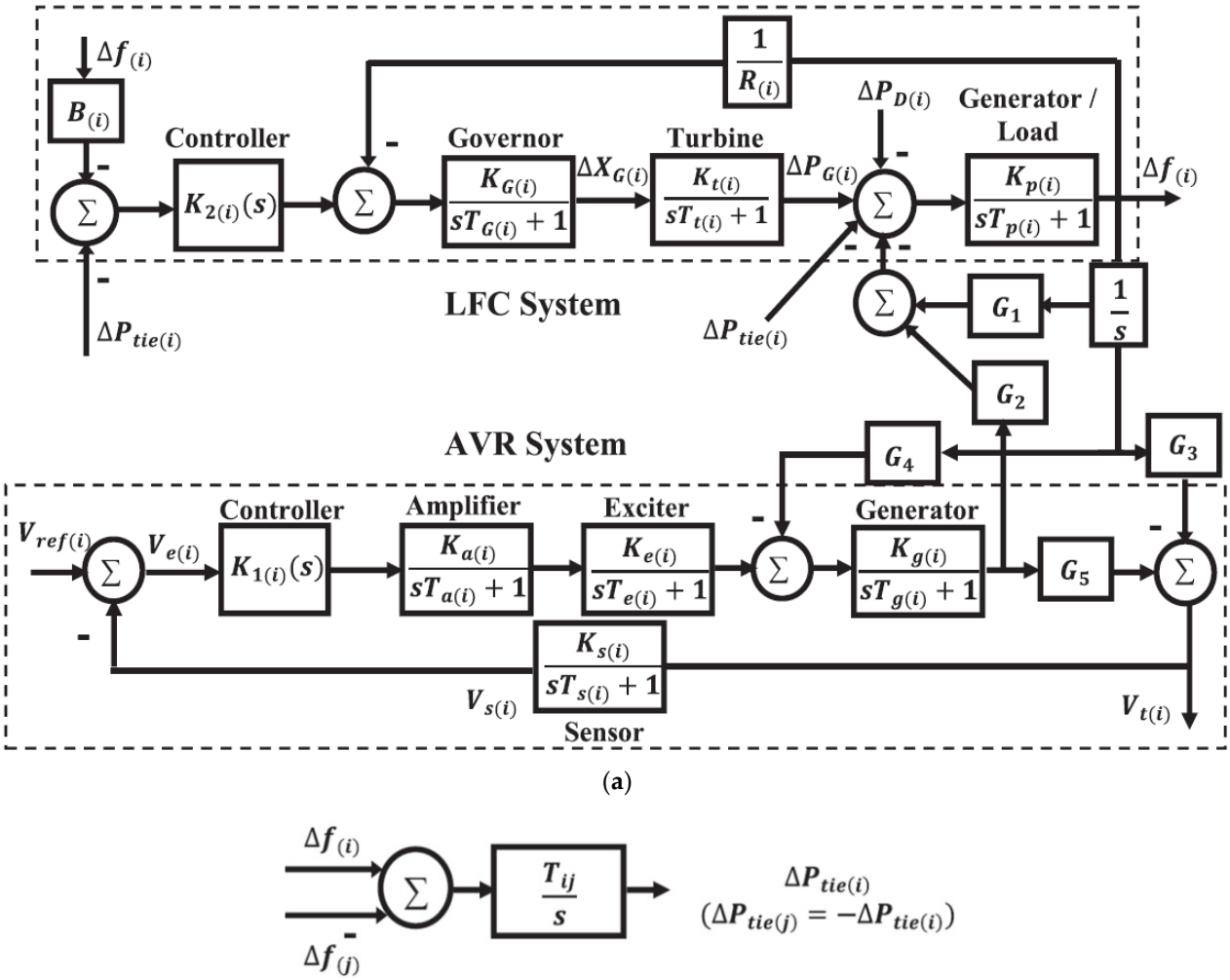

Figure 1. (**a**) Single-area AVR−LFC [5]. (**b**) Connections of two-area tie–line.

$V_{t(i)}$, $V_{e(i)}$, $V_{ref(i)}$, and $V_{s(i)}$ refer to the terminal output, error, reference, and sensor voltage in area-1, respectively. The AVR system of area-*i* consists of a controller ($K_{1(i)}(s)$), amplifier ($\frac{K_{a(i)}}{sT_{a(i)}+1}$), generator ($\frac{K_{g(i)}}{sT_{g(i)}+1}$), exciter ($\frac{K_{e(i)}}{sT_{e(i)}+1}$), and sensor ($\frac{K_{s(i)}}{sT_{s(i)}+1}$). Area-1′s LFC system has a controller $K_{2(i)}(s)$, turbine ($\frac{K_{t(i)}}{sT_{t(i)}+1}$), governor ($\frac{K_{G(i)}}{sT_{G(i)}+1}$), speed regulation ($R_i$), and generator/load ($\frac{K_{p(i)}}{sT_{p(i)}+1}$). $\Delta f_{(i)}$ denotes frequency deviation (Hz), $\Delta X_{G(i)}$ shows the valve position of the governor (p.u.MW),$\Delta P_{G(i)}$ represents the deviation in the output of the generator (p.u.MW), $\Delta P_{D(i)}$(p.u.MW) denotes the deviation in load, speed regulation is represented by $R_{(i)}$(Hz p.u.MW−1), and $\Delta P_{tie(i)}$ is the tie–line power. The purpose of tie–line is to interconnect multiple areas in IPS. Figure 1b shows the tie–line connections. The synchronization coefficient between area-*i* and area-*j* is represented by T_{ij}.

3. Proposed Control Methodology

The proportional integral derivative (PID) controller is commonly utilized in industrial applications owing to its easier implementation and simpler structure. The PID controller provides a satisfactory performance in most of the systems; however, the modified forms of the PID control structure have shown improved performance in many control systems, such as the AVR-LFC interconnected power system. The proportional integral–proportional derivative controller (PI-PD) is a modified version of PID, which is designed in such a way

to eliminate system errors with optimum transient and steady state response [43]. The PI part of PI-PD exists in a feed forward path and directly responds to the error signal coming from the summing junction. The PD part is located in the feedback path, and it is unaffected by sudden changes in the set point specification. The closed-loop response can be improved significantly with the addition of a controller part in the feedback path. The PI-PD controller has been successfully employed in the recent past in different applications [44–50]. The proposed control methodology with the combined LFC-AVR system is given in Figure 2. The transfer function of PI-PD controllers is represented as:

$$U(s) = (K_{p1} + \frac{K_i}{s})E(s) - (K_{p2} + K_d s)Y(s) \quad (1)$$

$$E(s) = Y(s) - R(s) \quad (2)$$

where $U(s)$, $Y(s)$, $R(s)$, and $E(s)$ denote the control, output, reference, and error signals, respectively. The cost function (J) is minimized to obtain the best possible parameters of the controllers. J depends upon $E(s)$, which is basically the difference between the output and reference signal.

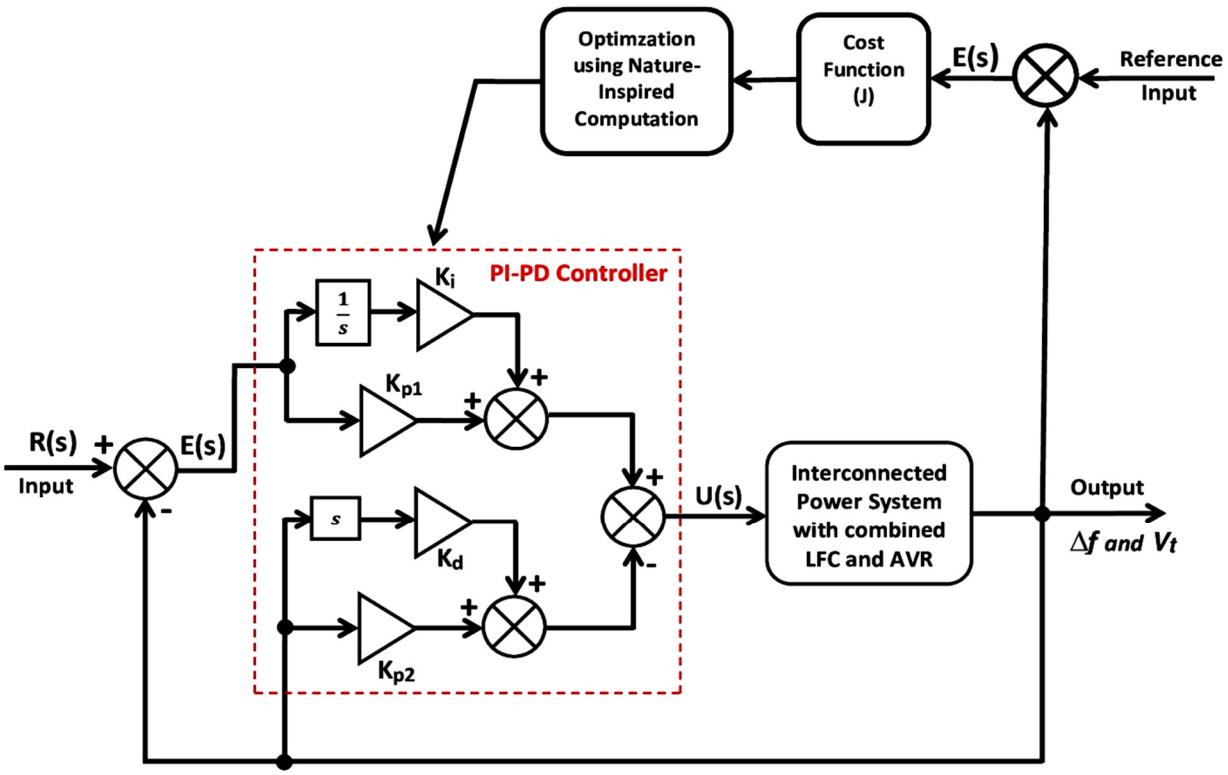

Figure 2. Proposed control methodology with combined LFC−AVR system.

In order to minimize the error signal, different types of performance indices can be used such as the integral of the squared value of the error signal (ISE), the integral of the time multiplied with the absolute value of the error signal (ITAE), the integral of the time multiplied with the squared value of the error signal (ITSE), and the integral of the absolute value of error (IAE) represented by the following equations:

$$J_{ISE,two-area} = \int_0^T [\Delta f_1^2 + \Delta f_2^2 + \Delta V_{t1}^2 + \Delta V_{t2}^2 + \Delta P_{tie12}^2]dt \quad (3)$$

$$J_{ITAE,two-area} = \int_0^T t[|\Delta f_1| + |\Delta f_2| + |\Delta V_{t1}| + |\Delta V_{t2}| + |\Delta P_{ptie12}|]dt \quad (4)$$

$$J_{ITSE,two-area} = \int_0^T t[\Delta f_1^2 + \Delta f_2^2 + \Delta V_{t1}^2 + \Delta V_{t2}^2 + \Delta P_{tie12}^2]dt \quad (5)$$

$$J_{IAE,two-area} = \int_0^T [|\Delta f_1| + |\Delta f_2| + |\Delta V_{t1}| + |\Delta V_{t2}| + |\Delta P_{ptie12}|]dt \quad (6)$$

For three-area IPS, we can write:

$$J_{ISE,three-area} = \int_0^T [\Delta f_1^2 + \Delta f_2^2 + \Delta f_3^2 + \Delta V_{t1}^2 + \Delta V_{t2}^2 + \Delta V_{t3}^2 + \Delta P_{tie1}^2 + \Delta P_{tie2}^2 + \Delta P_{tie3}^2]dt \quad (7)$$

$$J_{IAE,three-area} = \int_0^T [|\Delta f_1| + |\Delta f_2| + |\Delta f_3| + |\Delta V_{t1}| + |\Delta V_{t2}| + |\Delta V_{t3}| + |\Delta P_{ptie1}| + |\Delta P_{ptie2}| + |\Delta P_{ptie3}|]dt \quad (8)$$

$$J_{ITSE,three-area} = \int_0^T t[\Delta f_1^2 + \Delta f_2^2 + \Delta f_3^2 + \Delta V_{t1}^2 + \Delta V_{t2}^2 + \Delta V_{t3}^2 + \Delta P_{tie1}^2 + \Delta P_{tie2}^2 + \Delta P_{tie3}^2]dt \quad (9)$$

$$J_{ITAE,three-area} = \int_0^T t[|\Delta f_1| + |\Delta f_2| + |\Delta f_3| + |\Delta V_{t1}| + |\Delta V_{t2}| + |\Delta V_{t3}| + |\Delta P_{ptie1}| + |\Delta P_{ptie2}| + |\Delta P_{ptie3}|]dt \quad (10)$$

where,

$$\Delta V_{t1} = V_{ref} - V_{t1}\Delta V_{t2} = V_{ref} - V_{t2}\Delta V_{t3} = V_{ref} - V_{t3} \quad (11)$$

$$\Delta P_{ptie1} = \Delta P_{ptie12} + \Delta P_{ptie13}\Delta P_{ptie2} = \Delta P_{ptie21} + \Delta P_{ptie23}\Delta P_{ptie3} = \Delta P_{ptie31} + \Delta P_{ptie32} \quad (12)$$

When the cost function is minimized, the algorithm returns the best optimum parameters of the controller. To optimize the cost function (J), nature-inspired computation algorithms including LPBO, AOA, and MPSO were adapted.

4. Nature-Inspired Computation Algorithms

Due to their ability to solve complex valued problems, nature-inspired computation algorithms have gained brilliant attention in IPS. Keeping in view their remarkable contribution, an effort was made in this research to optimize the combined LFC and AVR-based IPS using nature-inspired computation techniques.

4.1. Learner Performance-Based Behavior Optimization

Rashid and Rahman presented a novel nature-inspired learner performance-based behavior optimization (LPBO) technique in 2020. The basic concept behind this algorithm is based on the fact that how students are admitted to different departments of a university is based on their high school performance. After admission, students must be able to improve their intellectual level to improve their skills. In this way, both exploitation and exploration phases are preserved. In this algorithm, a random population is generated with various ranges of grade point average (GPA). The applications of some of these learners will be rejected or accepted based on their fitness. After that, the population is divided in to subpopulation. Fitness is calculated and is then sorted into separate groups. The new population's structure is changed using crossover and mutation operators. A specified number of learners is acquired by different departments based on the minimum GPA criteria. This rejection and acceptance process is continued until all departments have their vacancies filled. Population fitness is improved in each iteration based on group learning, intellectual level, and teaching level [41]. Figure 3 presents the flow chart of the LPBO algorithm. Note that the LPBO population represents the PI-PD controller's parameters in this case.

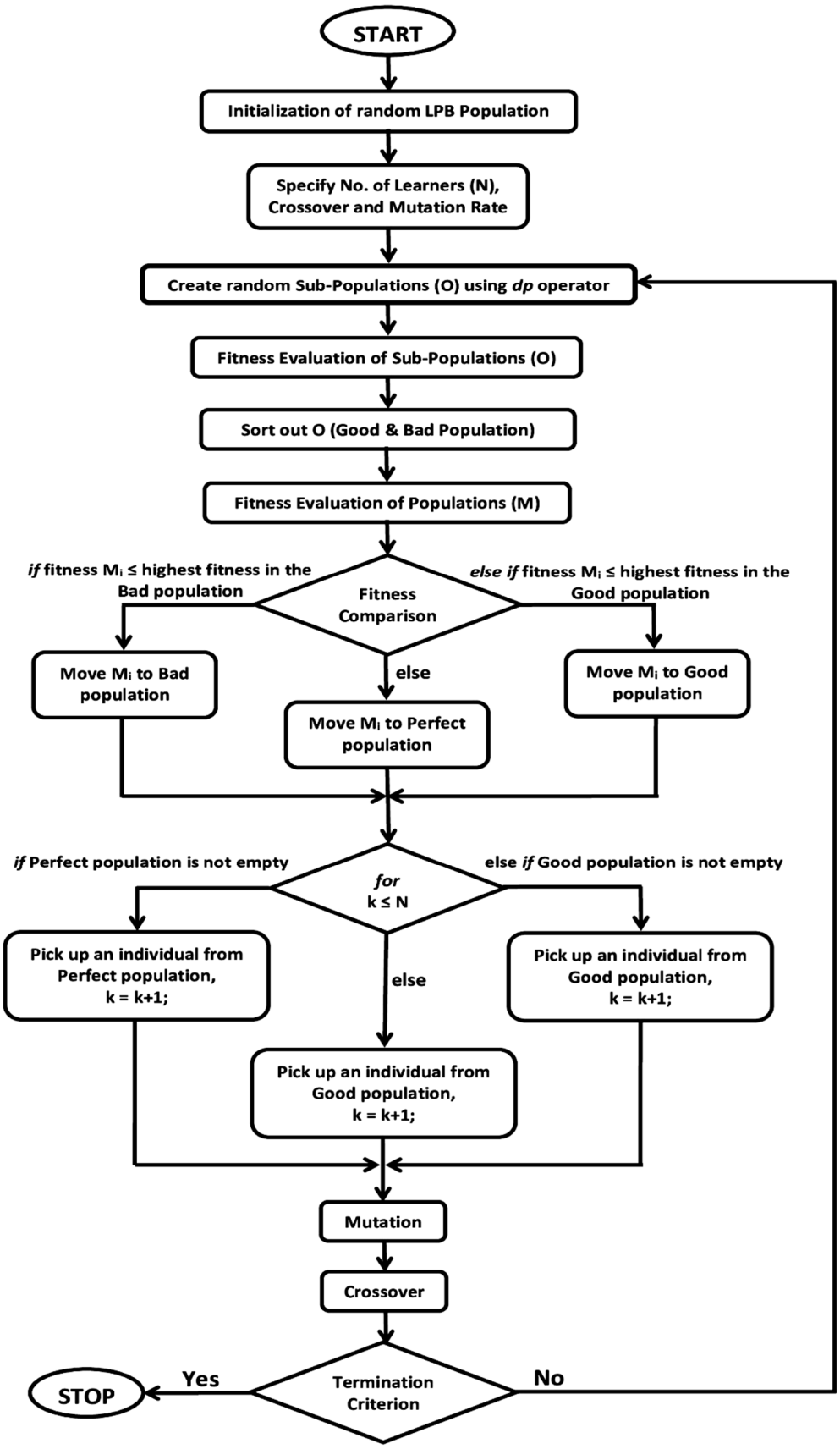

Figure 3. Flow chart of LPBO algorithm.

4.2. Archimedes Optimization Algorithm

The Archimedes optimization algorithm (AOA) is a new state-of-the-art algorithm based on the Archimedes principle. It deals with both convex and non-convex problems. It was invented in 2021 by Fatmaand Houssein. It defines the relationship between a buoyant force and an object submerged in water. The object will sink if the displaced fluid weight is less than the weight of the object. Similarly, if the displaced fluid and object weight are equal, the object floats on the fluid. An object has volume, acceleration, and density that results in the buoyancy force, as a result fluid's net force is always zero. AOA is a very effective nature-inspired algorithm in a way that it analyzes a problem with a global optimum solution. AOA fences in both exploitation and exploration phases since it is a global optimization algorithm. A comprehensive area must be examined to identify the global optimum solution of a given problem. Firstly, the fluid's random position is initialized, and then AOA evaluates the initial population fitness to discover the best possible solution until the selection criteria are met. The density and volume of each object changes at each AOA iteration. The new density, volume, and acceleration are obtained using the object's fitness. The AOA population represents the PI-PD controller's parameters [42]. Figure 4 presents a flow chart diagram of AOA.

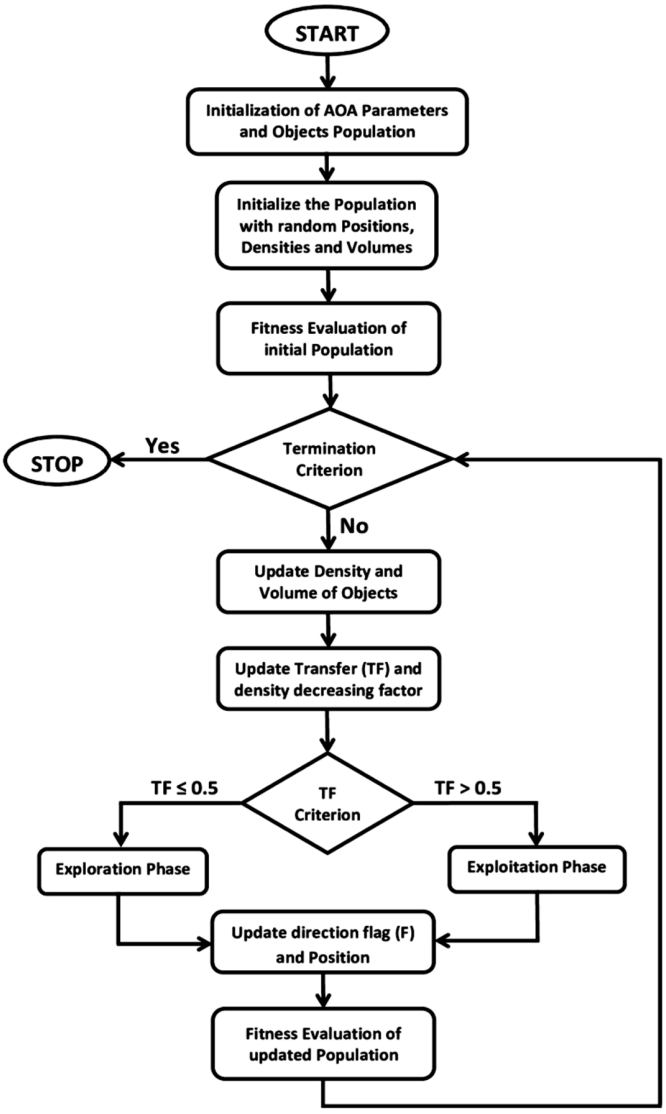

Figure 4. Flow chart of AOA.

4.3. Modified Particle Swarm Optimization (PSO)

Drawing inspiration from swarm intelligence, Eberhart and Kennedy proposed the particle swarm optimization (PSO) algorithm in 1995. In PSO, the movement of particles (candidate solutions) over a defined search space depends upon their velocity and position. The movement of particles is incited by the best possible positions known as local bests. These local bests lead particles toward the best possible position [51]. In modified particle swarm optimization (MPSO), the global learning coefficient is updated using a combination of existing local and global learning coefficients. The modification in the PSO algorithm is being made to improve the convergence characteristics of the controller. Figure 5 depicts the flow chart of the MPSO algorithm. Remember that in this research work, the particles represent the PI-PD controller's parameters.

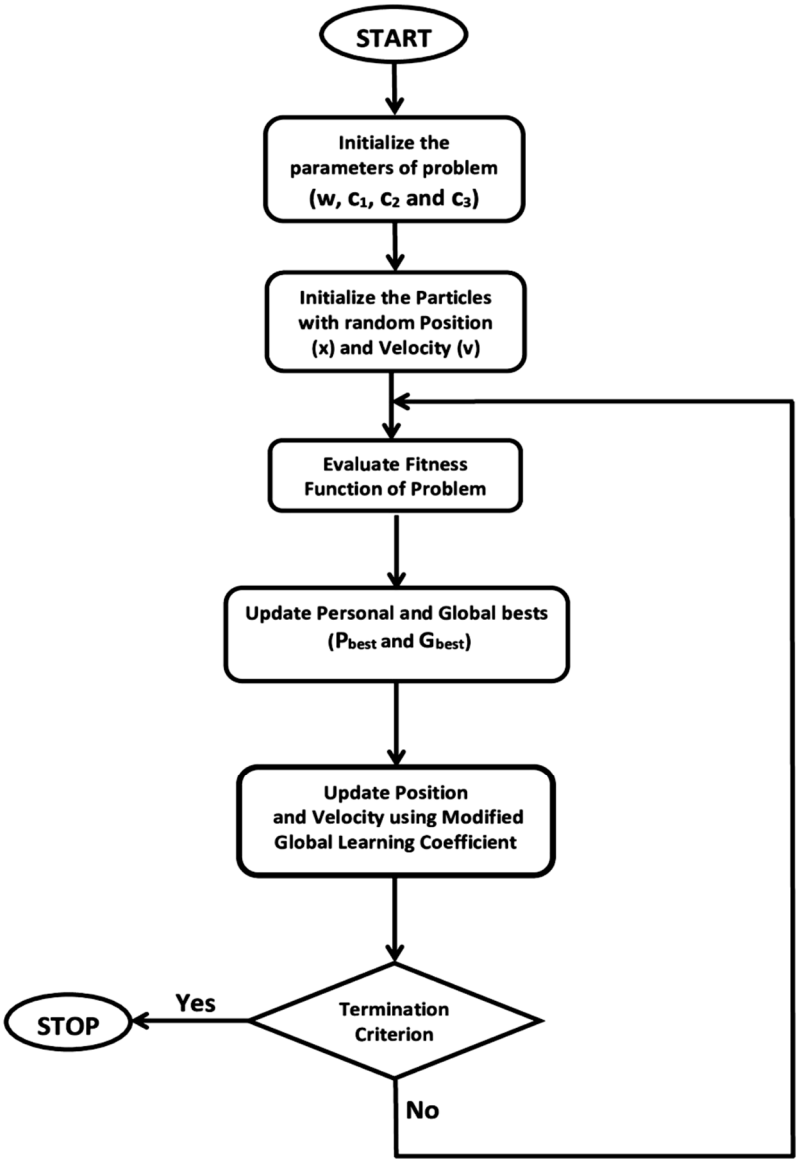

Figure 5. Flow chart of MPSO algorithm.

5. Implementation and Results Discussion

Multiple simulations were carried out in MATLAB/Simulink to express the validation of the proposed control methodology. Firstly, a two-area, two-source IPS with combined LFC and AVR was optimized using LPBO, AOA, and MPSO. ITSE was chosen as the error criterion, due to efficient error convergence characteristics. After achieving successful

results, the proposed methodology was applied to a three-area, three-source IPS with LFC-AVR loops.

5.1. Optimization of Two-Area Interconnected Power System

The two-area IPS model under investigation with a collective LFC-AVR system is shown in Figure 6. The system parameters of the two-area IPS are specified in Appendix A. The system parameters of area-1 and area-2 were chosen from [5] for a direct comparison of the proposed methodology with the NLTA-PID controller. The parameters of optimization algorithms such as MPSO, LPBO, and AOA used in simulations are given in Table 3. The tie–line connection between area-1 and are-2 can be established using Figure 7. The optimal parameters of MPSO-PI-PD, LPBO-PI-PD, and AOA-PI-PD control schemes are given in Table 4. For the sake of the assessment of the proposed control schemes, the evaluation of the time response of each schemes was carried out and comparisons were made with the results of NLTA-PID [5]. Further, a comparison between the proposed control schemes such as MPSO-PI-PD, LPBO-PI-PD, and AOA-PI-PD is also presented in detail in this section.

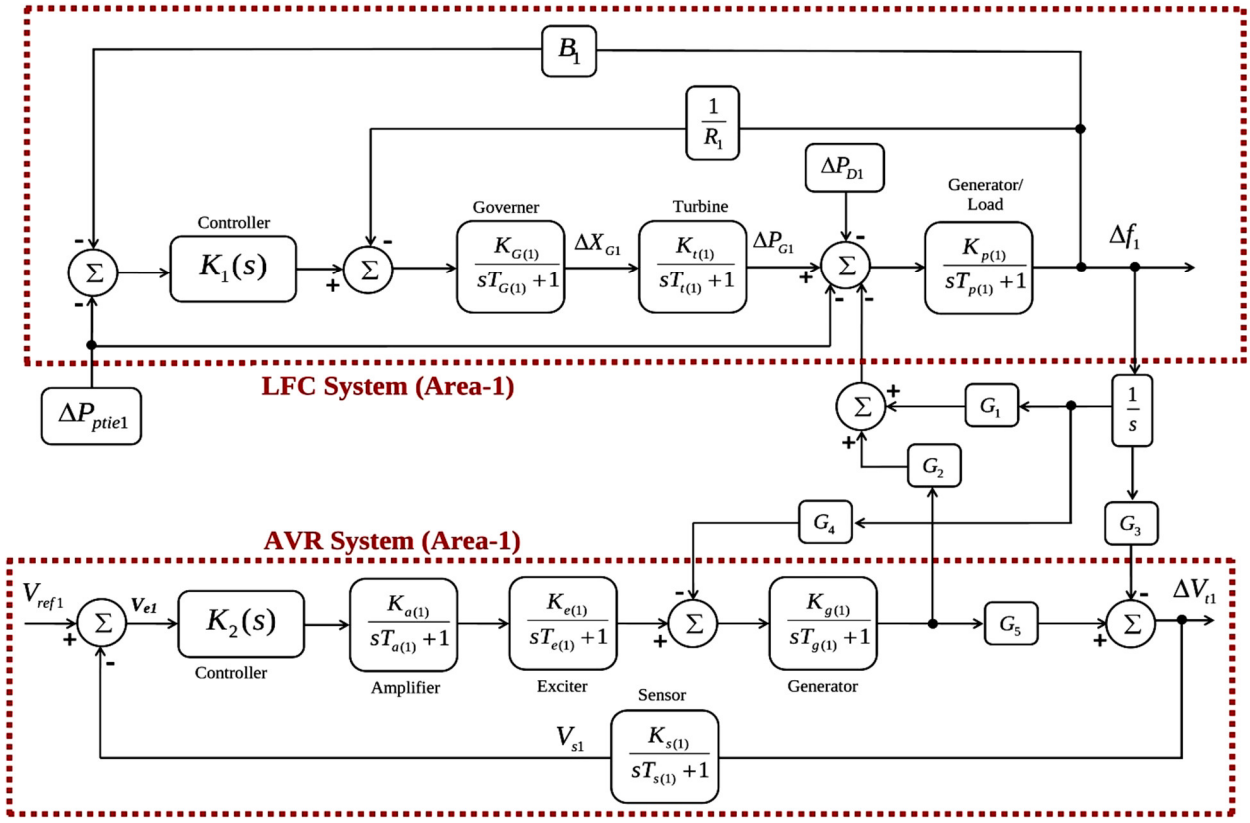

Figure 6. *Cont.*

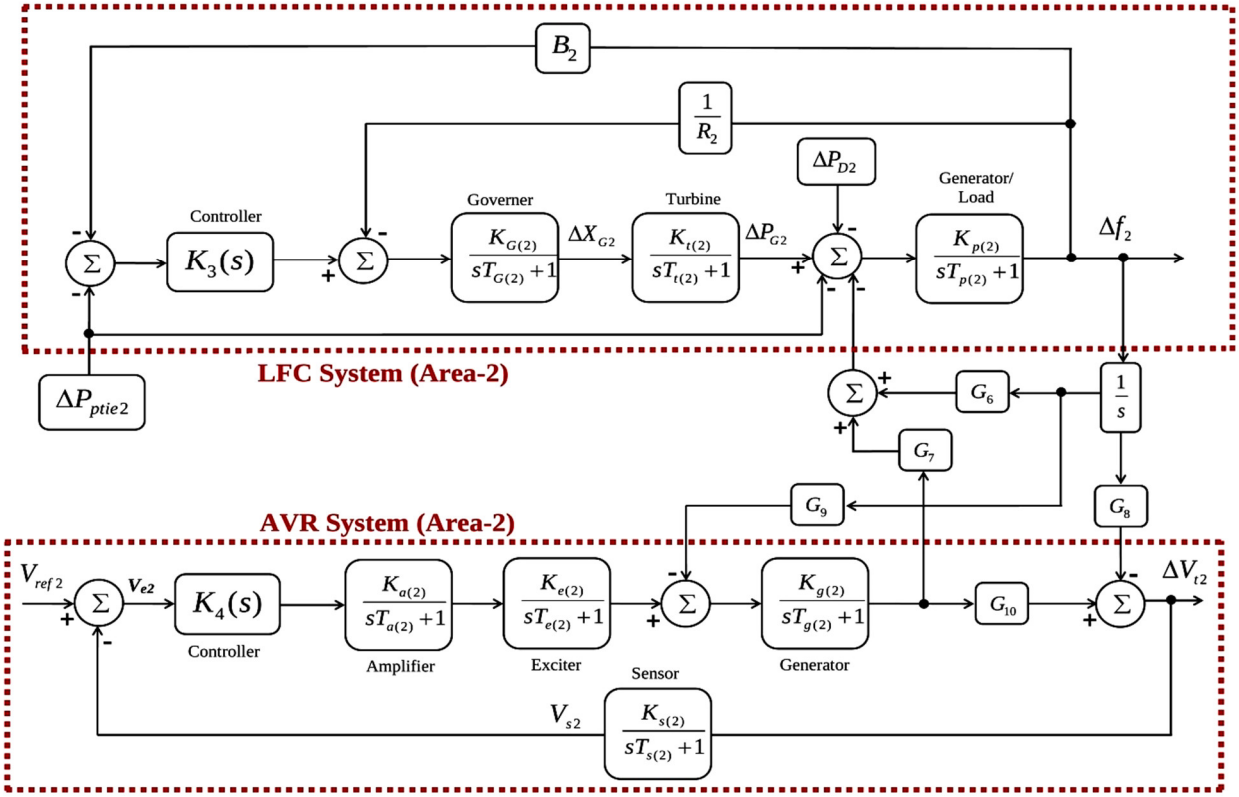

Figure 6. Two-area IPS with combined LFC−AVR.

Table 3. Parameters of optimization techniques.

MPSO		LPBO		AOA	
Parameter	Value	Parameter	Value	Parameter	Value
Population size	20	Population size	20	Population size	20
Iterations	10	Iterations	10	Iterations	10
Inertia Weight Damping Ratio	1	Crossover Percentage	0.7	C_1 (constant)	2
Personal Learning Coefficient	2.74	Mutation Percentage	0.3	C_2 (constant)	6
Global Learning Coefficient	2.88	Mutation Rate	0.03	C_3 (constant)	2
Max. Velocity Limit	0.2	Number of Mutants	6	C_4 (constant)	0.5
Min. Velocity Limit	−0.2	Number of Offspring	14	Range of Normalization (u,l)	0.9, 0.1

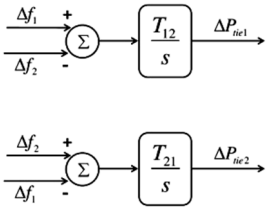

Figure 7. Tie–line connection.

Table 4. Optimal values of controller parameters (area-2).

Area	Controller Parameters	NLTA-PID [5]	Controller Parameters	Proposed Control Schemes		
				MPSO-PI-PD	LPBO-PI-PD	AOA-PI-PD
Area-1	K_{p1}	1.995	K_{p1}	1.061	1.064	1.61
	K_{i1}	1.943	K_{i1}	0.630	1.396	1.512
	K_{d1}	1.079	K_{p2}	1.162	1.071	1.88
	K_{p2}	1.994	K_{d1}	1.621	1.795	1.263
	K_{i2}	1.295	K_{p3}	1.063	1.850	1.01
	K_{d2}	1.107	K_{i2}	1.419	0.772	1.68
	-	-	K_{p4}	0.812	0.140	0.68
	-	-	K_{d2}	0.283	0.483	0.37
Area-2	K_{p3}	1.956	K_{p5}	0.564	0.965	0.90
	K_{i3}	1.919	K_{i3}	0.792	0.667	0.67
	K_{d3}	0.655	K_{p6}	0.775	0.670	1.44
	K_{p4}	1.283	K_{d3}	1.106	0.616	1.60
	K_{i4}	0.586	K_{p7}	1.903	1.522	1.50
	K_{d4}	0.819	K_{i4}	1.376	1.325	1.85
	-	-	K_{p8}	0.799	0.507	0.74
	-	-	K_{d4}	0.822	0.526	0.52
	ITSE	2.84	ITSE	0.250	0.164	0.1892

Figure 8 shows the frequency deviation curves of area-1 and area-2 using NLTA-PID [5], MPSO-PI-PD, LPBO-PI-PD, and AOA-PI-PD control techniques in a two-area IPS, respectively. It can be seen that the proposed control schemes provided a very satisfactory frequency deviation response. For the area-1 LFC, the settling time of NLTA-PID [5] was lower than the proposed schemes but at the cost of a high undershoot. NLTA-PID provided an undershoot of −0.285, whereas the proposed MPSO-PI-PD, LPBO-PI-PD, and AOA-PI-PD provided−0.130, −0.135, and −0.115, respectively. It can be noticed that the proposed MPSO-PI-PD, LPBO-PI-PD, and AOA-PI-PD provided 54%, 52.6%, and 60%, respectively, better undershoot responses as compared to the NLTA-PID controller in area-1. For area-2, NLTA-PD provided a quick settling, but it provided an undershoot of −0.275, whereas the proposed MPSO-PI-PD, LPBO-PI-PD, and AOA-PI-PD provided−0.135, −0.170, and −0.120, respectively. It was verified that the proposed MPSO-PI-PD, LPBO-PI-PD, and AOA-PI-PD provided 51%, 38%, and 56%, respectively, better undershoot responses as compared to the NLTA-PID controller. The percentages of overshoots and steady state (s-s) errors were almost zero with each proposed technique.

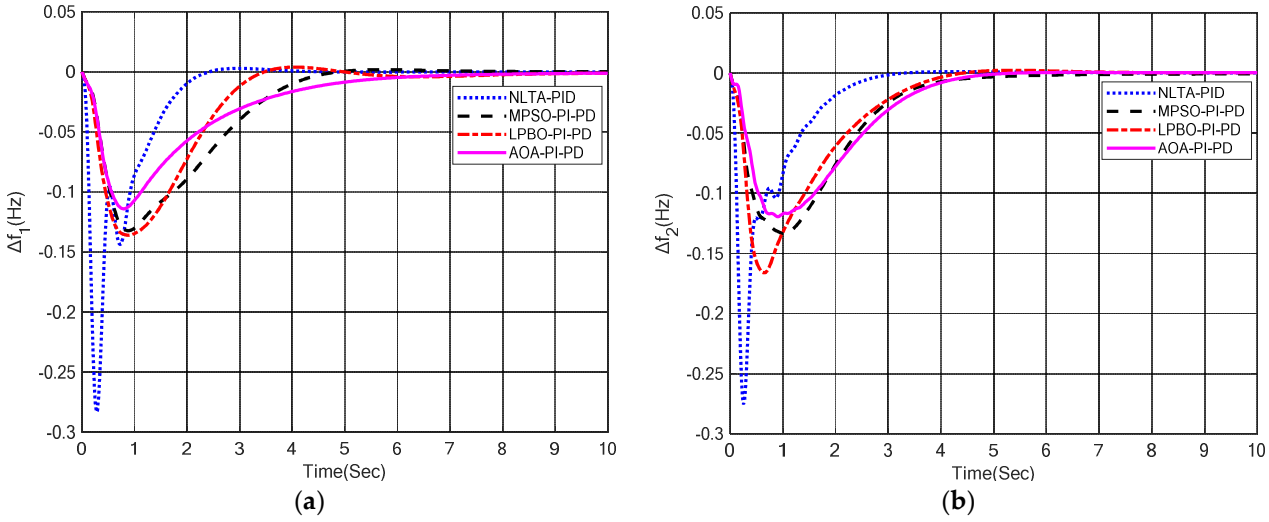

Figure 8. LFC response with PI−PD control scheme. (**a**) Δf_1; (**b**) Δf_2.

Figure 9 shows the terminal voltage of area-1 and area-2 using the NLTA-PID, MPSO-PI-PD, LPBO-PI-PD, and AOA-PI-PD control techniques in a two-area IPS, respectively. It is clear that the proposed control schemes provided a very satisfactory transient response in both area-1 and area-2. It is identified that NLTA-PID provided 18% and 17% overshoot in area-1 and area-2, respectively, but the proposed technique provided a negligible overshoot percentage at the cost of the settling time with all tuning techniques. It can be observed that the proposed LPBO-PI-PD and AOA-PI-PD control schemes produced settling times approximately the same as those achieved by NLTA-PID.

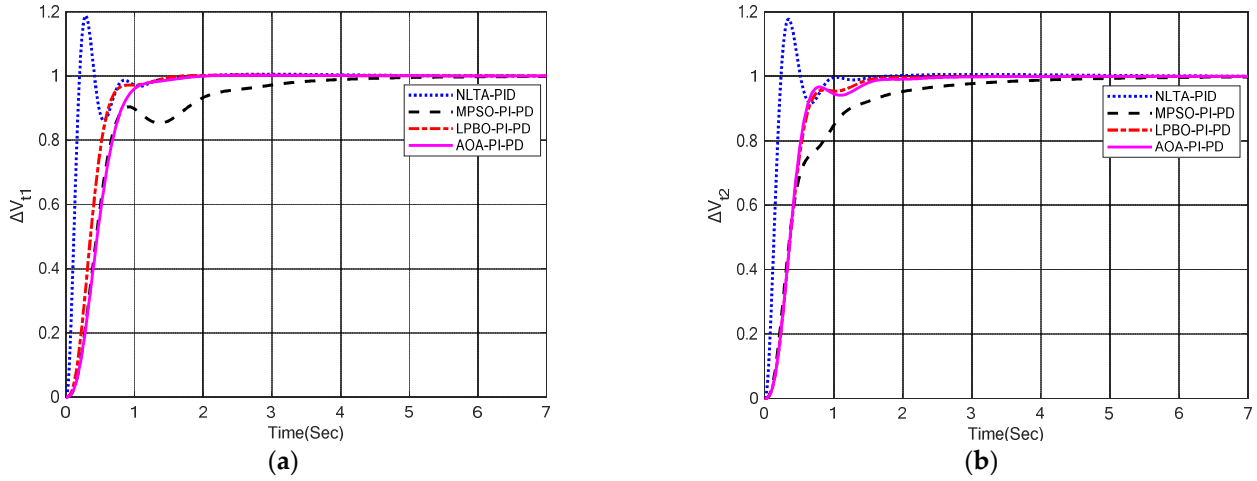

Figure 9. AVR response with PI-PD control scheme. (**a**) V_{t1}; (**b**) V_{t2}.

Figure 10 shows the tie–line power response using NLTA-PID, MPSO-PI-PD, LPBO-PI-PD, and AOA-PI-PD control techniques in a two-area IPS, respectively. It can be observed from the results that LPBO-PI-PD and AOA-PI-PD provided tie–line power responses with no undershoot; however, this was at the cost of a slightly small overshoot. In addition, the tie–line power responses yielded by MPSO-PI-PD, LPBO-PI-PD, and AOA-PI-PD were satisfactory.

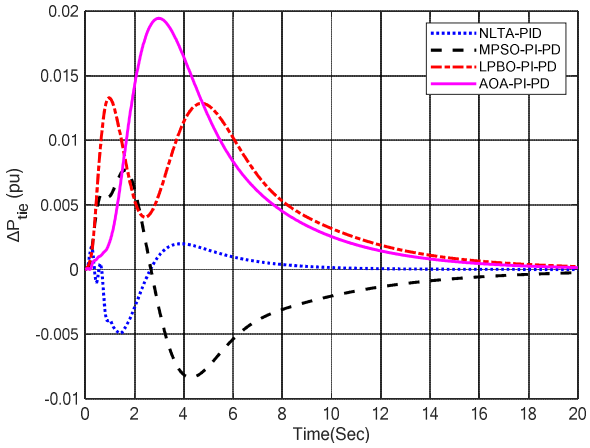

Figure 10. Tie–line power response in two−area IPS with combined LFC−AVR.

Tables 5 and 6 show the summary of LFC and AVR responses using NLTA-PID, MPSO-PI-PD, LPBO-PI-PD and AOA-PI-PD control schemes in a two-area IPS, respectively.

Table 5. LFC responses (area-2).

	Area-1				Area-2			
Control Scheme	**Settling Time**	**% Overshoot**	**Undershoot**	**s-s Error**	**Settling Time**	**% Overshoot**	**Undershoot**	**s-s Error**
NLTA-PID [5]	2.1204	0.0005	−0.285	0	2.592	0	−0.275	0
MPSO-PI-PD	4.5407	0	−0.13	0	4.92	0	−0.135	0
LPBO-PI-PD	6.9478	0.005	−0.135	0	4.043	0	−0.17	0
AOA-PI-PD	6.6752	0	−0.115	0	4.69	0	−0.12	0

Table 6. AVR responses (area-2).

Control Scheme	Area-1				Area-2			
	Rise Time	**Settling Time**	**% Overshoot**	**s-s Error**	**Rise Time**	**Settling Time**	**% Overshoot**	**s-s Error**
NLTA-PID [5]	0.1287	1.24	18.80	0	0.154	0.887	17.75	0
MPSO-PI-PD	0.6532	3.30	0	0	1.077	3.17	3.2971×10^{-4}	0
LPBO-PI-PD	0.4546	1.22	0.28	0	0.464	1.381	0	0
AOA-PI-PD	0.610	1.23	0.27	0	0.435	1.499	0	0

Figure 11 shows the graphical comparison of the performance parameters of NLTA-PID, MPSO-PI-PD, LPBO-PI-PD, and AOA-PI-PD control techniques in a two-area IPS, respectively. It is very clear that the proposed PI-PD control schemes provided relatively better responses in terms of the undershoot in LFC and overshoot percentage in AVR as compared to the NLTA-PID controller. From Tables 5 and 6 and Figure 11, it is concluded that the proposed MPSO-PI-PD, LPBO-PI-PD, and AOA-PI-PD were effective for maintaining the frequency and voltage within the prescribed values with a satisfactory performance in a two-area IPS.

5.2. Three-Area, Three-Source System

In this section, the proposed methodology is applied to a three-area IPS model with combined LFC-AVR. The model under study is presented in Figure 12, while the model parameters are provided in Appendix B.

The optimal values of MPSO-PI-PD, LPBO-PI-PD, and AOA-PI-PD for a three-area IPS with combined LFC and AVR are given in Table 7. Figure 13 shows the frequency deviation response using MPSO-PI-PD, LPBO-PI-PD, and AOA-PI-PD control techniques in a three-area IPS, respectively.

Table 7. Optimal values of controller parameters (area-3).

Area	**Controller Parameters**	**Proposed Control Schemes**		
		MPSO-PI-PD	**LPBO-PI-PD**	**AOA-PI-PD**
Area-1	K_{p1}	1.0995	0.66	1.51
	K_{i1}	1.1028	0.59	1.29
	K_{p2}	1.2737	0.96	−0.38
	K_{d1}	0.831	0.53	0.55
	K_{p5}	1.1106	0.77	0.86
	K_{i3}	0.9076	0.61	0.71
Area-2	K_{p6}	0.8639	1.48	1.55
	K_{d3}	1.3118	1.03	0.86
	K_{p7}	1.7917	1.68	1.91
	K_{i4}	1.8286	1.57	1.97
	K_{p8}	0.9068	0.83	1.074
	K_{d4}	0.6882	0.73	1.071

Table 7. *Cont.*

Area	Controller Parameters	Proposed Control Schemes		
		MPSO-PI-PD	LPBO-PI-PD	AOA-PI-PD
Area-3	K_{p3}	1.5371	1.56	0.88
	K_{i2}	1.965	1.62	1.91
	K_{p4}	1.2543	0.85	1.13
	K_{d2}	0.5936	0.56	0.5
	K_{p9}	0.7914	0.78	1.9
	K_{i5}	1.0795	1.12	1.26
	K_{p10}	1.2741	0.66	1.64
	K_{d5}	0.8581	1.56	0.42
	K_{p11}	1.2282	1.29	1.63
	K_{i6}	1.4326	1.3	1.69
	K_{p12}	0.9527	0.77	1.43
	K_{d6}	0.5874	0.45	1.33
	ITSE	0.3507	0.34485	0.4853

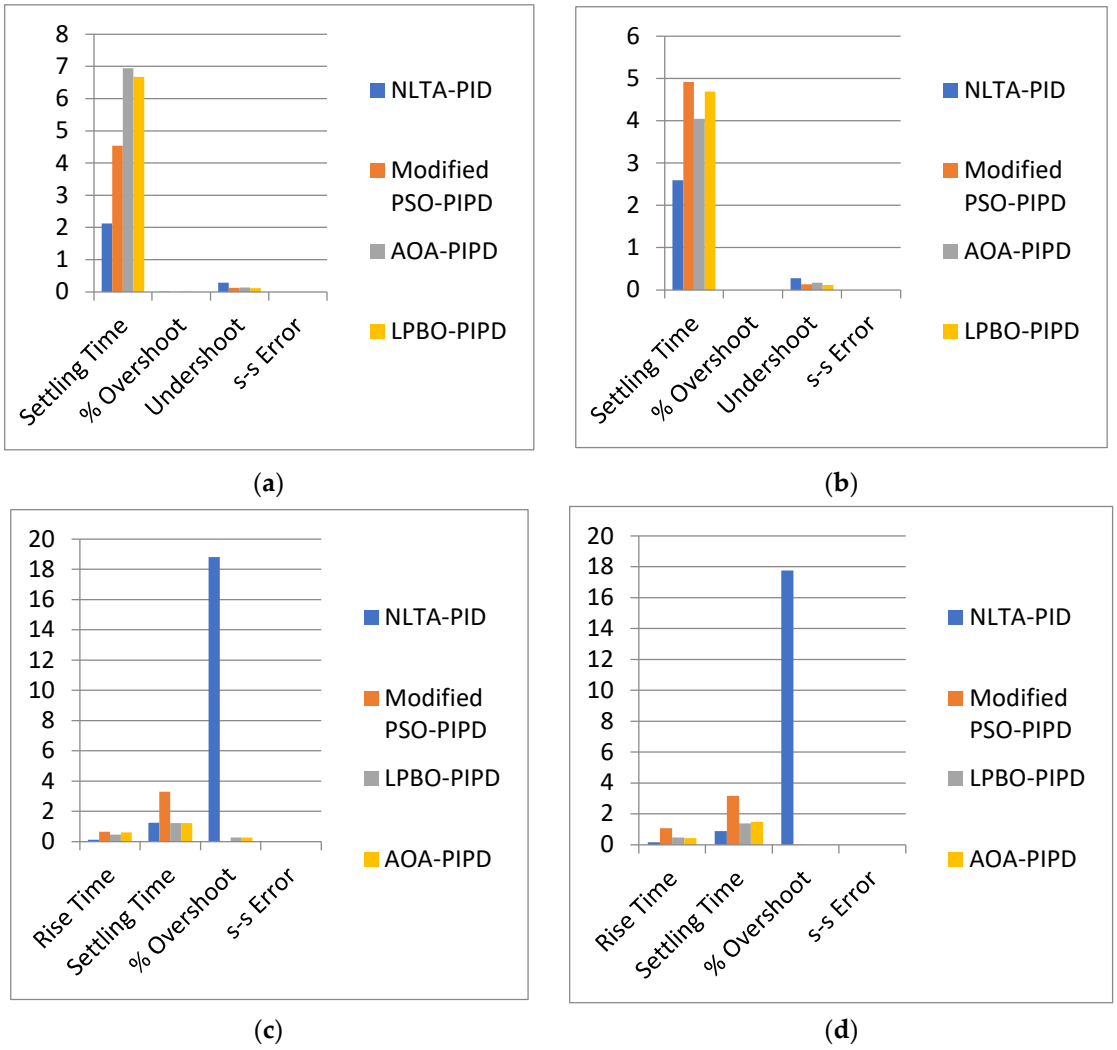

Figure 11. Graphical comparison of performance parameters. (**a**) Δf_1; (**b**) Δf_2; (**c**) V_{t1}; (**d**) V_{t2}.

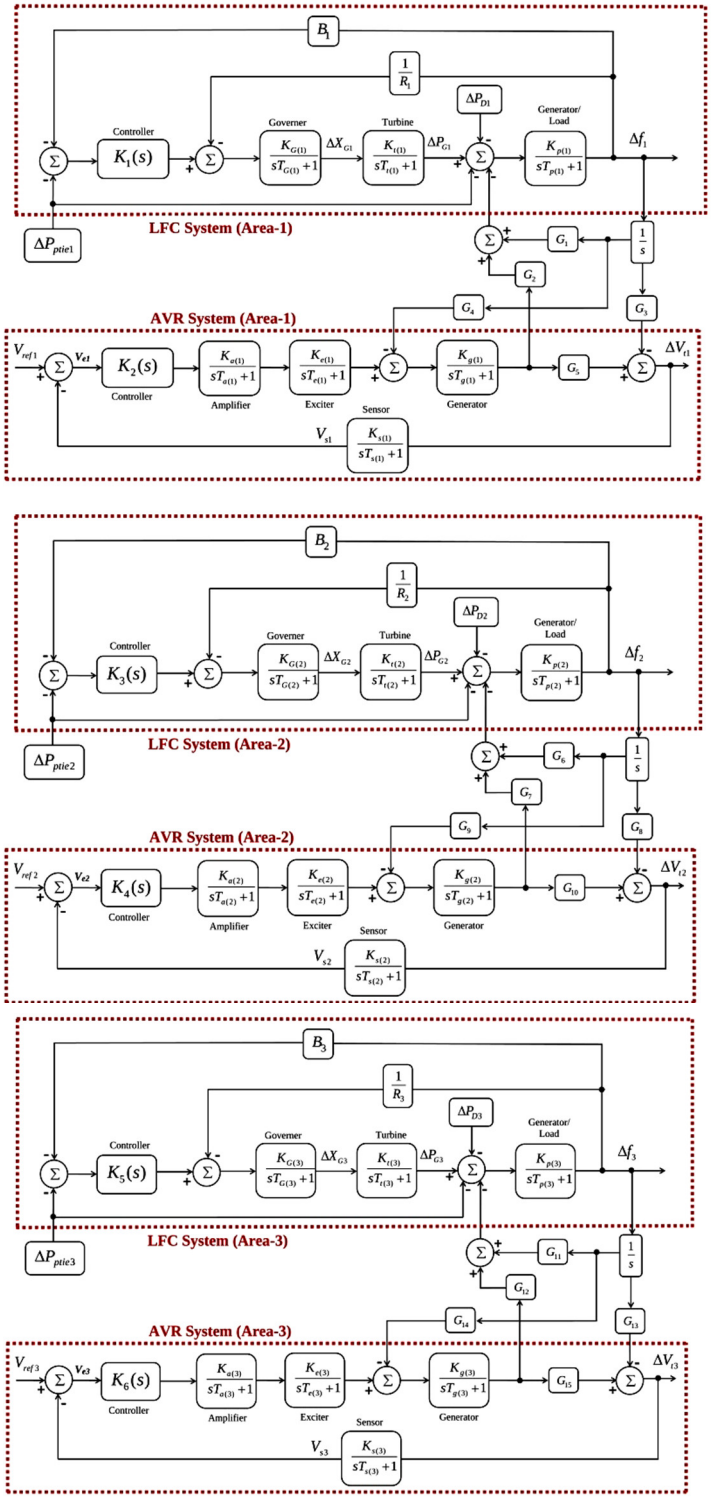

Figure 12. Three−area IPS with combined LFC−AVR.

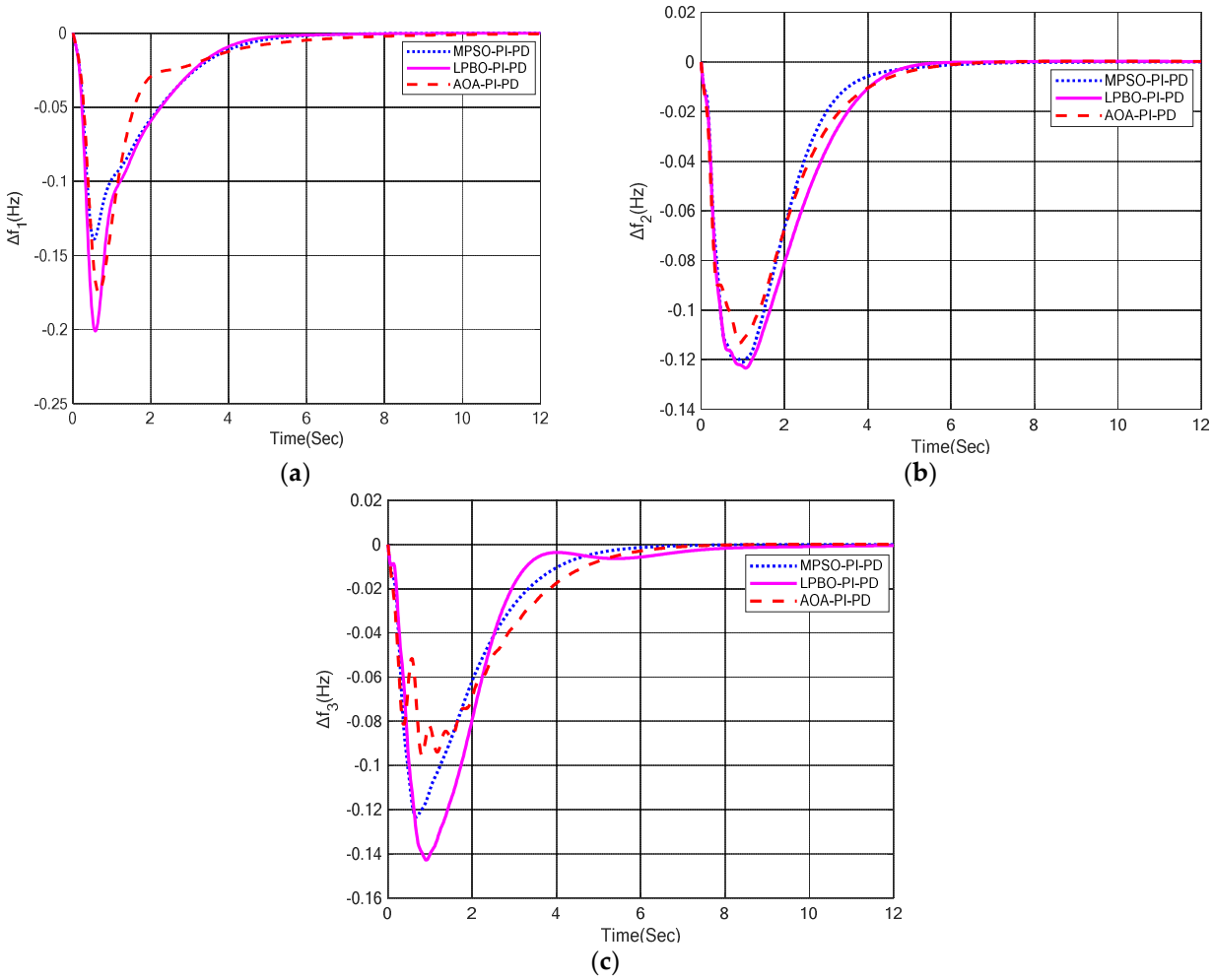

Figure 13. LFC response with PI−PD control scheme. (**a**) Δf_1; (**b**) Δf_2; (**c**) Δf_3.

Table 8 shows the summary of LFC responses of area-1, area-2, and area-3 using MPSO-PI-PD, LPBO-PI-PD, and AOA-PI-PD control techniques, respectively. For area-1, LPBO-PI-PD provided 14% and 31% quick settling times as compared to the MPSO-PI-PD and AOA-PI-PD control schemes, respectively. The overshoot percentage and steady state error were zero in each case.

Table 8. LFC responses (area-3).

Area	Control Scheme	Settling Time	% Overshoot	Undershoot	s-s Error
Area-1	MPSO-PI-PD	5.43	0	−0.14	0
	LPBO-PI-PD	4.65	0	−0.20	0
	AOA-PI-PD	6.73	0	−0.175	0
Area-2	MPSO-PI-PD	5.04	0	−0.120	0
	LPBO-PI-PD	4.87	0	−0.122	0
	AOA-PI-PD	5.46	0	−0.115	0
Area-3	PSO-PI-PD	5.40	0	−0.122	0
	LPBO-PI-PD	7.16	0	−0.143	0
	AOA-PI-PD	6.40	0	−0.095	0

Further, MPSO-PI-PD exhibited 30% and 20% better undershoot responses as compared to the LPBO-PI-PD and AOA-PI-PD control techniques, respectively. For area-2, LPBO-PI-PD yielded 3.3% and 11% quick settling times, as compared to the MPSO-PI-PD and AOA-PI-PD control schemes, respectively. The overshoot percentage and steady state

error were zero in each case. Further, AOA-PI-PD exhibited 4.16% and 5.74% better undershoot responses as compared to the MPSO-PI-PD and LPBO-PI-PD control schemes, respectively. For area-3, MPSO-PI-PD provided 25% and 16% quick settling times as compared to the LPBO-PI-PD and AOA-PI-PD control techniques, respectively. The overshoot percentage and steady state error were again zero in each case. Further, AOA-PI-PD exhibited 22% and 34% better undershoot responses as compared to the MPSO-PI-PD and LPBO-PI-PD control schemes, respectively. Figure 14 shows the terminal voltage responses of area-1, area-2, and area-3 using MPSO-PI-PD, LPBO-PI-PD, and AOA-PI-PD control techniques in a three-area IPS, respectively.

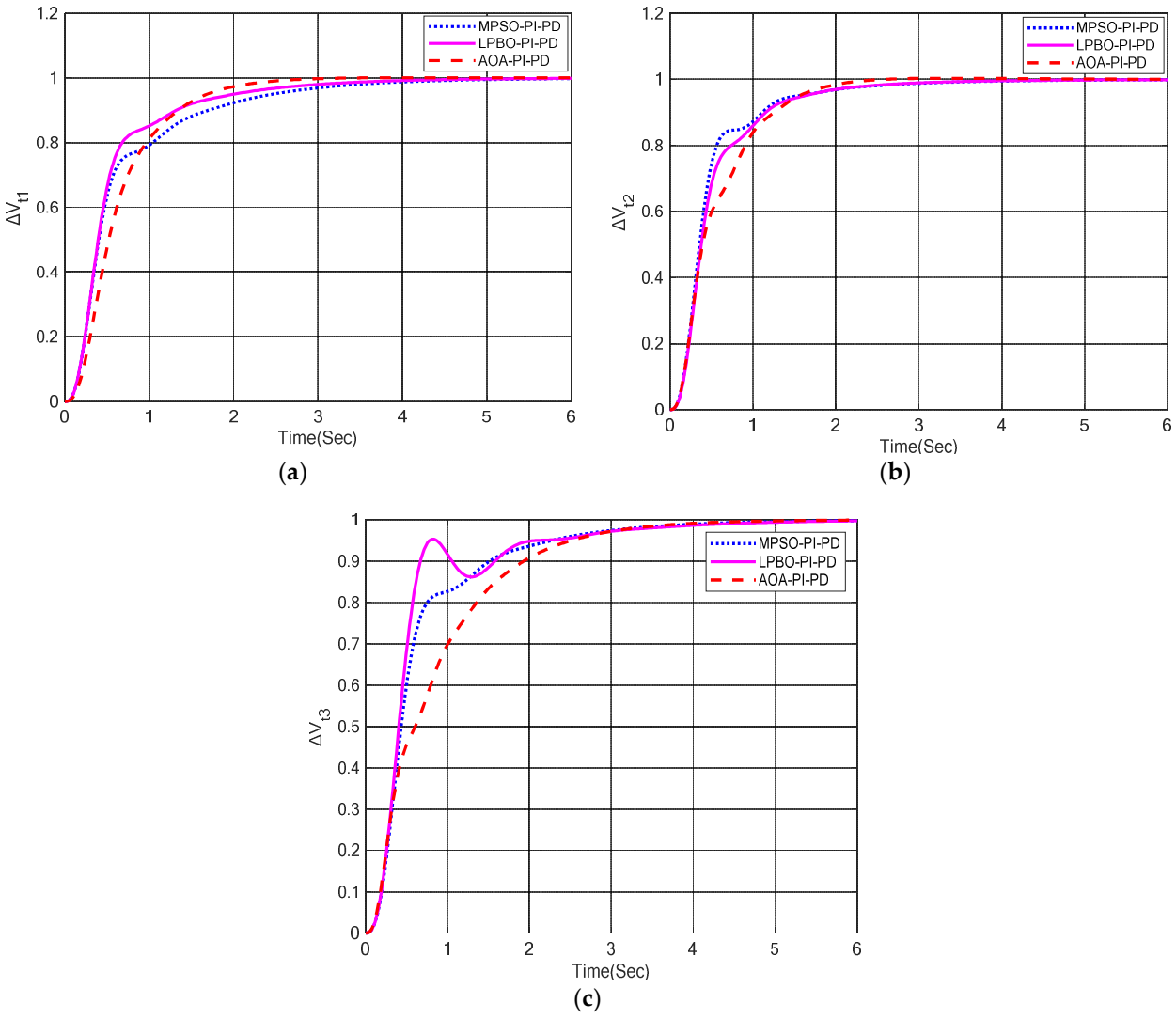

Figure 14. AVR response with PI-PD control scheme. (**a**) V_{t1}; (**b**) V_{t2}; (**c**) V_{t3}.

Table 9 shows the summary of AVR responses of area-1, area-2, and area-3 using the MPSO-PI-PD, LPBO-PI-PD, and AOA-PI-PD control schemes, respectively. For area-1, AOA-PI-PD provided 26% and 2% quick rise times as compared to the MPSO-PI-PD and LPBO-PI-PD control techniques, respectively. Moreover, AOA-PI-PD yielded 38% and 29% fast settling times as compared to the MPSO-PI-PD and LPBO-PI-PD control schemes, respectively. Further, it was observed that the percentage of overshoot and steady state error were almost zero with each tuning technique. For area-2, MPSO-PI-PD offered 3% and 13% quick rise times as compared to the LPBO-PI-PD and AOA-PI-PD control techniques, respectively. Moreover, AOA-PI-PD provided 21% and 19% fast settling times as compared to the MPSO-PI-PD and LPBO-PI-PD control schemes, respectively. Further, it can be seen

that the overshoot percentage and steady state error were almost zero with each tuning technique. For area-3, LPBO-PI-PD produced 64% and 73% quick rise times as compared to the MPSO-PI-PD and AOA-PI-PD control techniques, respectively. Moreover, AOA-PI-PD provided 0.3% and 5.45% fast settling times as compared to the MPSO-PI-PD and LPBO-PI-PD control schemes, respectively. Further, it can be seen that the overshoot percentage and steady state error were negligible with each tuning technique. Figure 15 shows the graphical comparison of the performance parameters of the MPSO-PI-PD, LPBO-PI-PD, and AOA-PI-PD control techniques in a three-area interconnected system.

Table 9. AVR responses (area-3).

Area	Control Scheme	Rise Time	Settling Time	% Overshoot	s-s Error
Area-1	MPSO-PI-PD	1.53	3.48	5.8225×10^{-6}	0
	LPBO-PI-PD	1.15	3.01	4.5973×10^{-4}	0
	AOA-PI-PD	1.13	2.15	0.083	0
Area-2	MPSO-PI-PD	0.95	2.44	0	0
	LPBO-PI-PD	0.98	2.37	0	0
	AOA-PI-PD	1.09	1.92	0.37	0
Area-3	MPSO-PI-PD	1.32	3.30	0	0
	LPBO-PI-PD	0.48	3.48	0.001	0
	AOA-PI-PD	1.75	3.29	0	0

Figure 16 shows the tie–line power responses of area-1, area-2, and area-3 using the MPSO-PI-PD, LPBO-PI-PD and AOA-PI-PD control schemes in a three-area IPS, respectively. It can be inferred that PI-PD-based control schemes including MPSO-PI-PD, LPBO-PI-PD, and AOA-PI-PD yielded satisfactory tie–line powers responses with negligible undershoots and overshoot percentages in the three-area IPS.

5.3. Sensitivity Analysis

In this section, the robustness of the proposed nature-inspired computation-based PI-PD control techniques were tested with large variations in the system parameters of the three-area IPS with combined LFC-AVR. The generator time constant (T_g) and turbine time constant (T_t) were varied to $\hat{A} \pm 50\%$ of their nominal values. The newer values of T_g and T_t after $\hat{A} \pm 50\%$ variations are given in Appendix B. The optimum parameters of the PI-PD control scheme were the same as those used in Case 2. The AVR and LFC responses of the PI-PD control scheme with variations in T_t and T_g are depicted in Figures 17 and 18, respectively. Tables 10 and 11 show the summary of the performance parameters of LFC and AVR responses under parametric variations. From the obtained results, it is evident the overshoot percentages and steady state error were almost zero in each case. The AVR responses are almost indistinguishable to each other, despite the variation in system parameters. Figure 19 shows the graphical comparison of the performance parameters under this scenario. It is clearly observed that the system response under $\hat{A} \pm 50\%$ variations was very identical to response with nominal values. This indicates that the proposed LPBO-PI-PD control technique was very realistic and robust under variations in the system parameters. These results clearly reveal that the re-tuning of the proposed controller is not necessary with large variations of at least $\hat{A} \pm 50\%$.

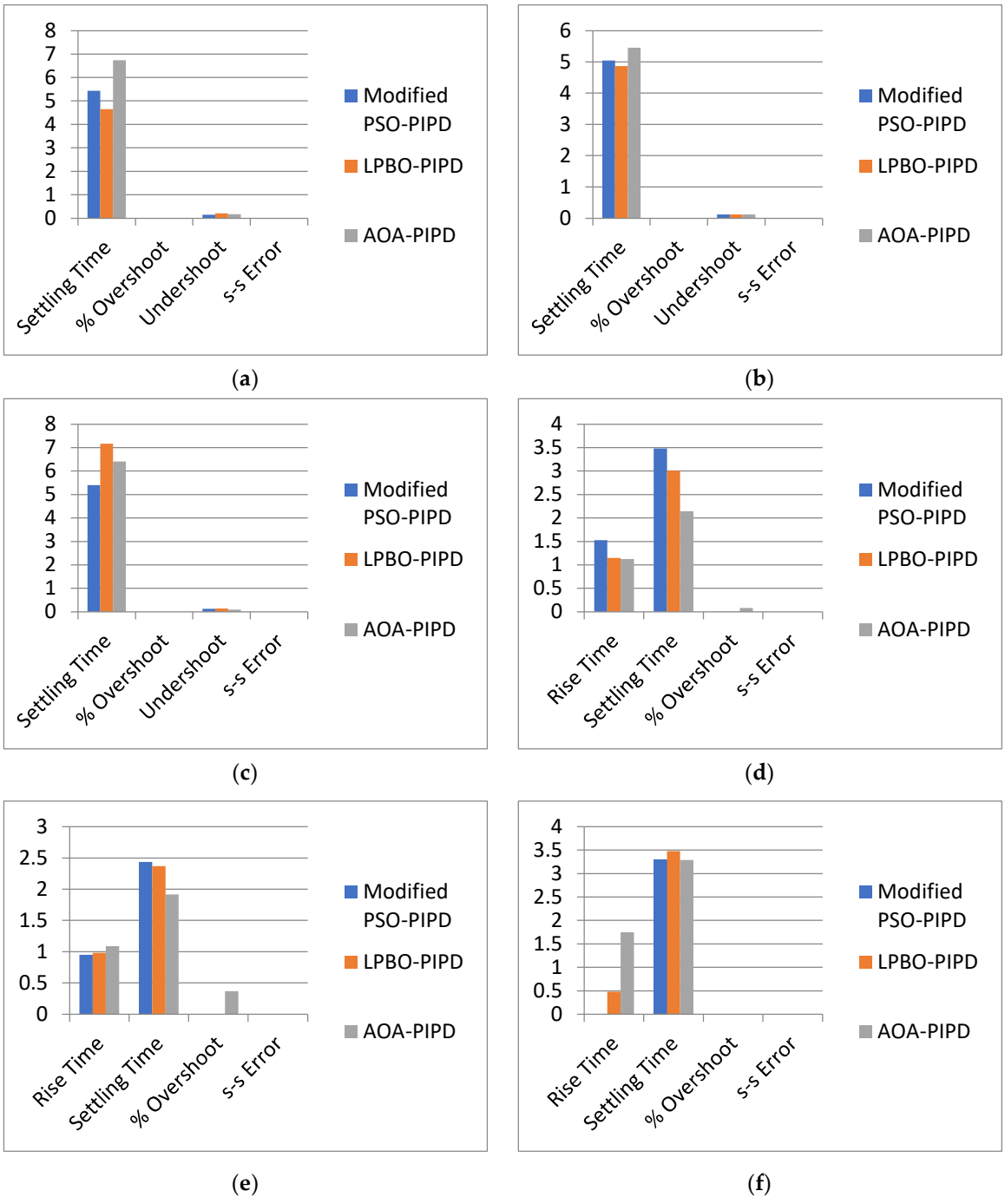

Figure 15. Graphical comparison of performance parameters. (**a**) Δf_1; (**b**) Δf_2; (**c**) Δf_3;(**d**) V_{t1}; (**e**) V_{t2}; (**f**) V_{t3}.

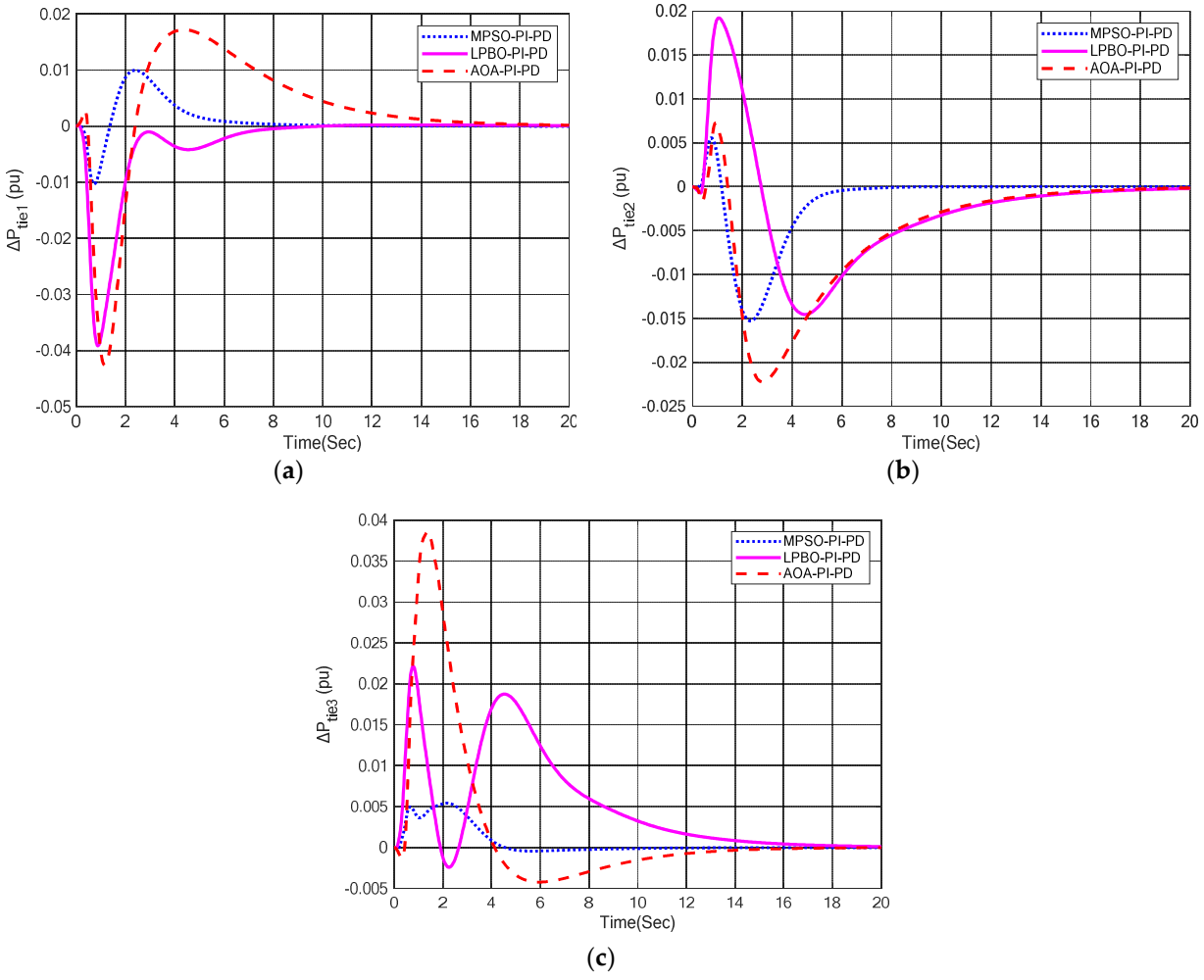

Figure 16. Tie−line power responses with PI−PD control scheme. (**a**) ΔP_{tie1}; (**b**) ΔP_{tie2}; (**c**) ΔP_{tie3}.

Table 10. Settling time responses of PI-PD control scheme with variations in system parameters.

Parameters/Variation	**Settling Time (LFC and AVR)**					
	Δf_1	Δf_2	Δf_3	V_{t1}	V_{t2}	V_{t3}
Nominal T_g, T_t	4.65	4.87	7.16	3.01	2.37	3.48
T_{g1}, T_{g2}, $T_{g3/}$+50%	4.60	4.76	7.02	2.74	2.11	3.56
T_{g1}, T_{g2}, $T_{g3/}$−50%	4.71	4.95	7.32	3.25	2.59	3.56
T_{t1}, T_{t2}, $T_{t3/}$+50%	4.63	5.01	7.18	3.03	2.38	3.48
T_{t1}, T_{t2}, $T_{t3/}$−50%	4.60	4.71	7.11	2.99	2.36	3.48

Table 11. Overshoot and undershoot responses of PI-PD control scheme with variations in system parameters.

Parameters/Variation	**%Overshoot (LFC and AVR)**						**%Undershoot (LFC)**		
	Δf_1	Δf_2	Δf_3	V_{t1}	V_{t2}	V_{t3}	Δf_1	Δf_2	Δf_3
Nominal T_g, T_t	0	0	0	0	0	0	−0.2	−0.122	−0.143
T_{g1}, T_{g2}, $T_{g3/}$+50%	0	0	0	0	0	3.4	−0.185	−0.13	−0.155
T_{g1}, T_{g2}, $T_{g3/}$−50%	0	0	0	0	0	0	−0.215	−0.125	−0.13
T_{t1}, T_{t2}, $T_{t3/}$+50%	0	0	0	0	0	0	−0.245	−0.125	−0.15
T_{t1}, T_{t2}, $T_{t3/}$−50%	0	0	0	0	0	0	−0.16	−0.125	−0.135

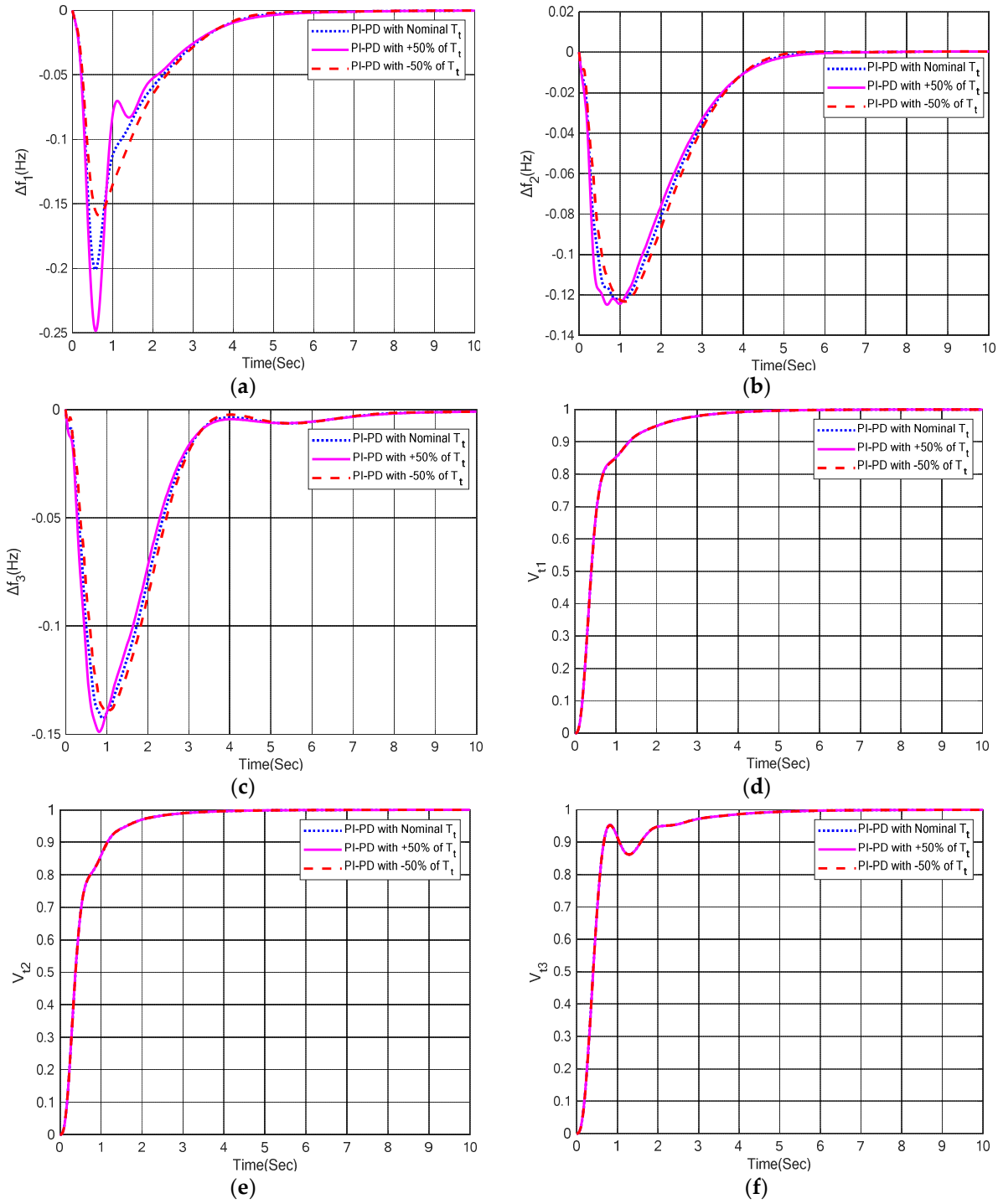

Figure 17. LFC and AVR responses with variations in T_t. (**a**) Δf_1 in area−1; (**b**) Δf_2 in area−2; (**c**) Δf_3 in area−3; (**d**) V_{t1} in area−1; (**e**) V_{t2} in area−2 and (**f**) V_{t3} in area−3.

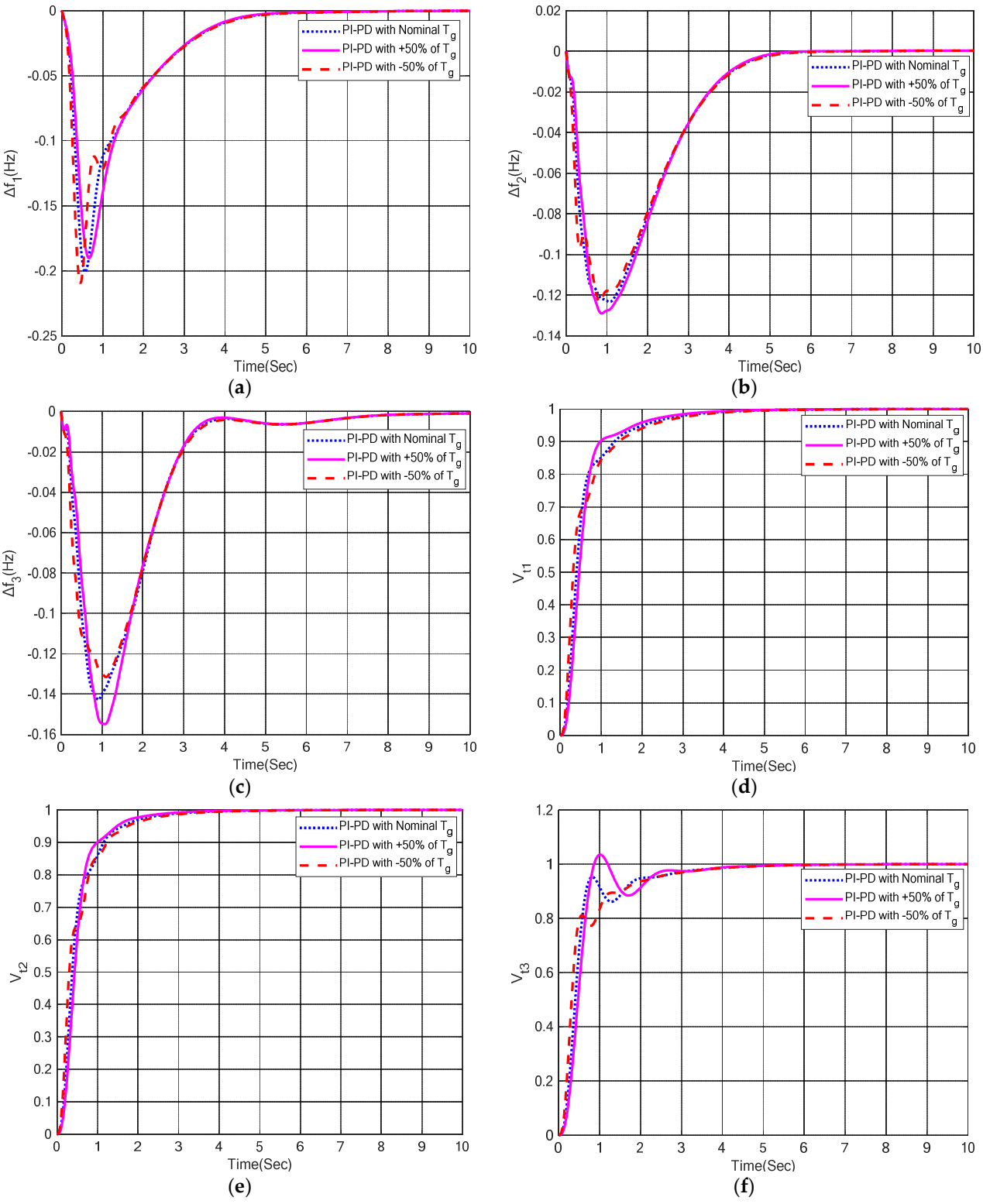

Figure 18. LFC and AVR responses with variations in T_g. (**a**) Δf_1 in area−1; (**b**) Δf_2 in area−2; (**c**) Δf_3 in area−3; (**d**) V_{t1} in area−1; (**e**) V_{t2} in area−2 and (**f**) V_{t3} in area−3.

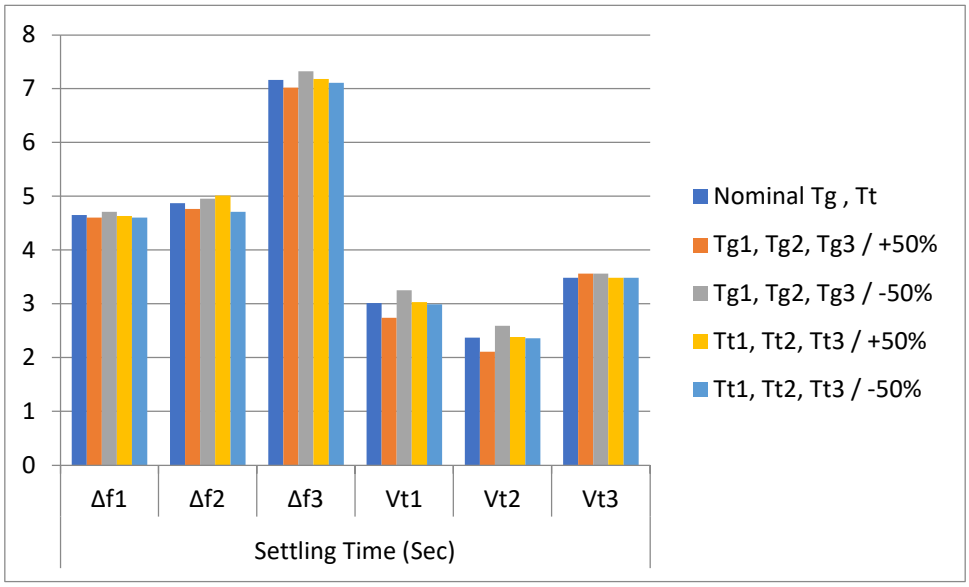

(**a**)

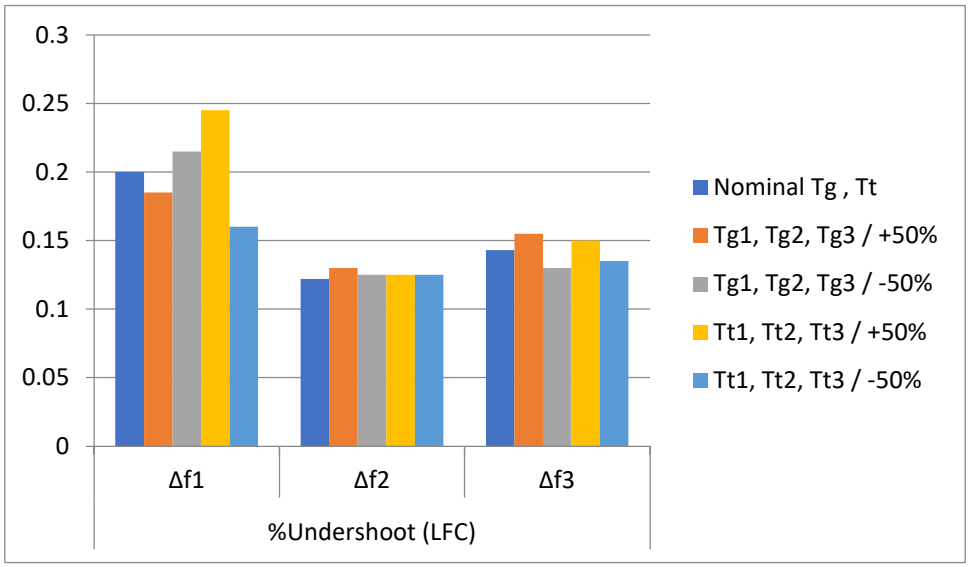

(**b**)

Figure 19. Graphical comparison of performance parameters in three-area IPS with variations in T_g and T_t. (**a**) Settling time; (**b**) undershoot.

6. Conclusions and Future Work

The multi-area IPS included numerous control areas, which are connected through the AC tie–line. The transient and steady state performance of a multi-area IPS with AVR-LFC was thoroughly investigated in this research.Nature-inspired computation including MPSO-, LPBO-, and AOA-based PI-PD control technique was proposed for the optimization of the multi-area system. From the findings of Case 1, it is concluded that all proposed schemes provided relatively better undershoot responses as compared to the NLTA-PID controller [5] for LFC. Particularly, the AOA-PI-PD control scheme exhibited 60% and 56% better undershoots in the area-1 and area-2 LFC, respectively, as compared to the NLTA-PID controller. Similarly, NLTA-PID provided 18% and 17% overshoot in the area-1 and area-2 AVR, respectively, but the proposed PI-PD control scheme completely eliminated the overshoot percentage with each tuning algorithm. The results of Case 2 reveal that LPBO-PI-PD provided 14% and 31% quick settling times in area-1, whereas 3.3% and

11% quick settling times were provided in the area-2 LFC as compared to the MPSO-PI-PD and AOA-PI-PD control techniques, respectively. In the area-3 LFC, MPSO-PI-PD provided relatively lower settling times (25% and 16%) as compared to the LPBO-PI-PD and AOA-PI-PD control schemes, respectively. MPSO-PI-PD provided relatively better undershoot (30% and 20%) in the area-1 LFC, whereas the AOA-PI-PD control technique provided better undershoot in the area-1 (4.16% and 5.74%) and area-2 (22% and 34%) LFC, respectively. Moreover, the AOA-PI-PD control scheme provided 26% and 2% quick rise times, and 38% and 29% fast settling times in the area-1 AVR as compared to the MPSO-PI-PD and LPBO-PI-PD control schemes, respectively. Further, MPSO-PI-PD provided 3% and 13% fast rise times in the area-2 AVR as compared to the LPBO-PI-PD and AOA-PI-PD control schemes, respectively. AOA-PI-PD provided 21% and 19% quick settling times in the area-2 AVR, and 0.3% and 5.45% fast settling times in the area-3 AVR as compared to the MPSO-PI-PD and AOA-PI-PD control schemes, respectively. For the area-3 AVR, LPBO-PI-PD provided 64% and 73% fast rise times as compared to the MPSO-PI-PD and AOA-PI-PD control schemes, respectively. Finally, the resilience of the PI-PD control technique was assessed by varying the system parameters (Â $\pm$ 50%), and a comprehensive sensitivity analysis was carried out to confirm its robustness. The results confirm the superiority of the proposed PI-PD control scheme when applied to multi-area IPS with combined LFC and AVR. Keeping in mind the value of the present work, IPS with a combined LFC-AVR can be analyzed by incorporating multi-source and various energy storage devices to enhance the dynamic response of the power systems. Further, neuro-fuzzy and hybrid ANN controllers can also be utilized for multi-area multi-sources IPS. It will be worth employing PI-PD, neuro-fuzzy, or hybrid ANN to multi-area IPS under nonlinearity constraints. Moreover, very recently introduced nature-inspired computing techniques such as dandelion optimization, artificial rabbits optimization, and sea-horse optimization can be explored to find the optimal parameters of controllers in such types of application.

Author Contributions: Conceptualization, T.A., S.A.M., A.T.A.; Data curation, T.A., S.A.M., A.D., H.M.; Formal analysis, T.A., S.A.M., A.D., H.M., A.T.A., I.A.H.; Investigation, A.T.A., I.A.H.; Methodology, T.A., S.A.M., A.D., H.M., A.T.A., I.A.H.; Project administration, A.T.A., I.A.H.; Resources, T.A., S.A.M., A.D., H.M.; Supervision, A.T.A., I.A.H.; Validation, T.A., S.A.M., A.D., H.M.; Visualization, A.D., H.M., A.T.A., I.A.H.; Writing—original draft, T.A., S.A.M., A.D., H.M.; Writing—review & editing, T.A., S.A.M., A.D., H.M., A.T.A., I.A.H.; Funding Acquisition, I.A.H. All authors have read and agreed to the published version of the manuscript.

Funding: This research was funded by Norwegian University of Science and Technology.

Institutional Review Board Statement: Not applicable.

Informed Consent Statement: Not applicable.

Acknowledgments: The authors would like to acknowledge the support of Norwegian University of Science and Technology for paying the Article Processing Charges (APC) of this publication. Special acknowledgment to Automated Systems & Soft Computing Lab (ASSCL), Prince Sultan University, Riyadh, Saudi Arabia. In addition, the authors wish to acknowledge the editor and anonymous.

Conflicts of Interest: The authors declare no conflict of interest.

Appendix A

Table A1. Area-2 [5].

Sr. No.	Area-1		Area-2	
	System's Parameter	Value	System's Parameter	Value
1	B_1	1	B_2	1
2	R_1	2.4	R_2	1.2
3	K_{G1}	1	K_{G2}	1

Table A1. *Cont.*

Sr. No.	Area-1		Area-2	
	System's Parameter	Value	System's Parameter	Value
4	T_{G1}	0.08	T_{G2}	0.12
5	K_{t1}	1	K_{t2}	1
6	T_{t1}	0.3	T_{t2}	0.15
7	ΔP_{D1}	0.02	ΔP_{D2}	0.02
8	K_{p1}	120	K_{p2}	100
9	T_{p1}	20	T_{p2}	10
10	K_{a1}	10	K_{a2}	10
11	T_{a1}	0.1	T_{a2}	0.1
12	K_{e1}	1	K_{e2}	1.5
13	T_{e1}	0.4	T_{e2}	0.6
14	K_{g1}	1	K_{g2}	1.5
15	T_{g1}	1	T_{g2}	1.5
16	K_{s1}	1	K_{s2}	1
17	T_{s1}	0.01	T_{s2}	0.01
18	G_1	1.5	G_6	1.5
19	G_2	0.3	G_7	0.3
20	G_3	0.1	G_8	0.1
21	G_4	1.4	G_9	1.4
22	G_5	0.5	G_{10}	0.5
23	T_{12}	0.545	T_{21}	0.545

Appendix B

Table A2. System parameters of area-1, area-2, and area-3.

Sr. No.	Area-1		Area-2		Area-3	
	System's Parameter	Value	System's Parameter	Value	System's Parameter	Value
1	B_1	1	B_2	1	B_3	1
2	R_1	2.4	R_2	1.20	R_3	1.20
3	K_{G1}	1	K_{G2}	1	K_{G3}	1
4	T_{G1}	0.08	T_{G2}	0.12	T_{G3}	0.12
5	K_{t1}	1	K_{t2}	1	K_{t3}	1
6	T_{t1}	0.3	T_{t2}	0.15	T_{t3}	0.15
7	ΔP_{D1}	0.02	ΔP_{D2}	0.02	ΔP_{D3}	0.02
8	K_{p1}	120	K_{p2}	100	K_{p3}	100
9	T_{p1}	20	T_{p2}	10	T_{p3}	10
10	K_{a1}	10	K_{a2}	10	K_{a3}	10
11	T_{a1}	0.1	T_{a2}	0.1	T_{a3}	0.1
12	K_{e1}	1	K_{e2}	1.5	K_{e3}	1.8
13	T_{e1}	0.4	T_{e2}	0.6	T_{e3}	0.8
14	K_{g1}	1	K_{g2}	1.5	K_{g3}	1.8
15	T_{g1}	1	T_{g2}	1.5	T_{g3}	1.8
16	K_{s1}	1	K_{s2}	1	K_{s3}	1
17	T_{s1}	0.01	T_{s2}	0.01	T_{s3}	0.01
18	G_1	1.5	G_6	1.5	G_{11}	1.5
19	G_2	0.3	G_7	0.3	G_{12}	0.3
20	G_3	0.1	G_8	0.1	G_{13}	0.1
21	G_4	1.4	G_9	1.4	G_{14}	1.4
22	G_5	0.5	G_{10}	0.5	G_{15}	0.5
23	T_{12}	0.545	T_{21}	0.545	T_{31}	0.545
24	T_{13}	0.545	T_{23}	0.545	T_{32}	0.545

Table A3. System parameters after Â ± 50% variations in T_g and T_t.

Sr. No.	Area-1		Area-2		Area-3	
	System's Parameter	Value	System's Parameter	Value	System's Parameter	Value
1	T_{g1} (+50%)	1.5	T_{g2} (+50%)	2.25	T_{g3} (+50%)	2.7
	T_{g1} (Nominal)	1	T_{g2} (Nominal)	1.5	T_{g3} (Nominal)	1.8
	T_{g1} (−50%)	0.5	T_{g2} (−50%)	0.75	T_{g3} (−50%)	0.9
2	T_{t1} (+50%)	0.45	T_{t2} (+50%)	0.225	T_{t3} (+50%)	0.225
	T_{t1} (Nominal)	0.3	T_{t2} (Nominal)	0.15	T_{t3} (Nominal)	0.15
	T_{t1} (−50%)	0.15	T_{t2} (−50%)	0.075	T_{t3} (−50%)	0.075

References

1. Kalyan, C.N.S.; Goud, B.S.; Reddy, C.R.; Bajaj, M.; Sharma, N.K.; Alhelou, H.H.; Siano, P.; Kamel, S. Comparative Performance Assessment of Different Energy Storage Devices in Combined LFC and AVR Analysis of Multi-Area Power System. *Energies* **2022**, *15*, 629. [CrossRef]
2. Ghosh, A.; Ray, A.K.; Nurujjaman; Jamshidi, M. Voltage and frequency control in conventional and PV integrated power systems by a particle swarm optimized Ziegler–Nichols based PID controller. *SN Appl. Sci.* **2021**, *3*, 1–13. [CrossRef]
3. Prakash, A.; Parida, S.K. Combined Frequency and Voltage Stabilization of Thermal-Thermal System with UPFC and RFB. In Proceedings of the 2020 IEEE 9th Power India International Conference (PIICON), Sonepat, India, 28 February–1 March 2020; pp. 1–6. [CrossRef]
4. Fayek, H.H.; Rusu, E. Novel Combined Load Frequency Control and Automatic Voltage Regulation of a 100% Sustainable Energy Interconnected Microgrids. *Sustainability* **2022**, *14*, 9428. [CrossRef]
5. Nahas, N.; Abouheaf, M.; Sharaf, A.M.; Gueaieb, W. A Self-Adjusting Adaptive AVR-LFC Scheme for Synchronous Generators. *IEEE Trans. Power Syst.* **2019**, *34*, 5073–5075. [CrossRef]
6. Gupta, A.; Chauhan, A.; Khanna, R. Design of AVR and ALFC for single area power system including damping control. In Proceedings of the 2014 Recent Advances in Engineering and Computational Sciences (RAECS 2014), Chandigarh, India, 6–8 March 2014; pp. 6–8. [CrossRef]
7. Chandrashekar, M.J.; Jayapal, R. AGC and AVR implementation in a deregulated power system using optimized controller with Renewable integrated DC link. In Proceedings of the 2019 1st International Conference on Advanced Technologies in Intelligent Control, Environment, Computing & Communication Engineering (ICATIECE 2019), Bangalore, India, 19–20 March 2019; pp. 355–364. [CrossRef]
8. Rajbongshi, R.; Saikia, L.C. Coordinated performance of interline power flow controller and superconducting magnetic energy storage in combined ALFC and AVR system under deregulated environment. *J. Renew. Sustain. Energy* **2018**, *10*, 044102. [CrossRef]
9. Kalyan, C.N.S.; Rao, G.S. Combined frequency and voltage stabilisation of multi-area multisource system by DE-AEFA optimised PID controller with coordinated performance of IPFC and RFBs. *Int. J. Ambient Energy* **2020**, 1–17. [CrossRef]
10. Kalyan, C.N.S.; Rao, G.S. Frequency and voltage stabilisation in combined load frequency control and automatic voltage regulation of multiarea system with hybrid generation utilities by AC/DC links. *Int. J. Sustain. Energy* **2020**, *39*, 1009–1029. [CrossRef]
11. Sahani, A.K.; Raj, U.; Shankar, R.; Mandal, R.K. Firefly Optimization Based Control Strategies for Combined Load Frequency Control and Automatic Voltage Regulation for Two-Area Interconnected Power System. *Int. J. Electr. Eng. Inform.* **2019**, *11*, 747–758. [CrossRef]
12. Lal, D.K.; Barisal, A.K. Combined load frequency and terminal voltage control of power systems using moth flame optimization algorithm. *J. Electr. Syst. Inf. Technol.* **2019**, *6*, 1–24. [CrossRef]
13. Grover, H.; Verma, A.; Bhatti, T.S. Load frequency control & automatic voltage regulation for a single area power system. In Proceedings of the 2020 IEEE 9th Power India International Conference (PIICON 2020), Sonepat, India, 28 February–1 March 2020; pp. 1–5. [CrossRef]
14. Salman, G.; Jafar, A.S.; Ismael, A.I. Application of artificial intelligence techniques for LFC and AVR systems using PID controller. *Int. J. Power Electron. Drive Syst. (IJPEDS)* **2019**, *10*, 1694–1704. [CrossRef]
15. Kouba, N.E.Y.; Menaa, M.; Hasni, M.; Boudour, M. Optimal control of frequency and voltage variations using PID controller based on Particle Swarm Optimization. In Proceedings of the 2015 4th International Conference on Systems and Control (ICSC), Sousse, Tunisia, 28–30 April 2015; pp. 424–429. [CrossRef]
16. Safiullah, S.; Rahman, A.; Lone, S.A. State-observer based IDD controller for concurrent frequency-voltage control of a hybrid power system with electric vehicle uncertainties. *Int. Trans. Electr. Energy Syst.* **2021**, *31*, e13083. [CrossRef]
17. Mohammadikia, R.; Nikoofard, A.; Tavakoli-Kakhki, M. Application of MPC for an automatic voltage regulator and load frequency control of interconnected power system. In Proceedings of the 2020 28th Iranian Conference on Electrical Engineering (ICEE), Tabriz, Iran, 4–6 August 2020. [CrossRef]
18. Eke, I.; Saka, M.; Gozde, H.; Arya, Y.; Taplamacioglu, M.C. Heuristic optimization based dynamic weighted state feedback approach for 2DOF PI-controller in automatic voltage regulator. *Eng. Sci. Technol. Int. J.* **2021**, *24*, 899–910. [CrossRef]

19. Wagle, R.; Sharma, P.; Sharma, C.; Gjengedal, T.; Pradhan, C. Bio-inspired hybrid BFOA-PSO algorithm-based reactive power controller in a standalone wind-diesel power system. *Int. Trans. Electr. Energy Syst.* **2021**, *31*. [CrossRef]
20. Prasad, S.; Purwar, S.; Kishor, N. Load frequency regulation using observer based non-linear sliding mode control. *Int. J. Electr. Power Energy Syst.* **2018**, *104*, 178–193. [CrossRef]
21. Panigrahi, N.; Nayak, A.; Mishra, S.R. Morphology of the Alumina Nanoparticles for the Arrangement of the KF Stacked Nano–γ–Al2O3 as Catalyst for Conversion of Biomass to Fuel. In *Advances in Energy Technology*; Springer: Berlin/Heidelberg, Germany, 2021; pp. 125–132.
22. Daraqz, A.; Malik, S.A.; Waseem, A.; Azar, A.T.; Haq, I.U.; Ullah, Z.; Aslam, S. Automatic generation control of multi-source interconnected power system using FOI-TD controller. *Energies* **2021**, *14*, 5867. [CrossRef]
23. Guo, J. Application of a novel adaptive sliding mode control method to the load frequency control. *Eur. J. Control* **2020**, *57*, 172–178. [CrossRef]
24. Arya, Y.; Kumar, N. Design and analysis of BFOA-optimized fuzzy PI/PID controller for AGC of multi-area traditional/restructured electrical power systems. *Soft Comput.* **2016**, *21*, 6435–6452. [CrossRef]
25. Daraz, A.; Malik, S.A.; Mokhlis, H.; Haq, I.U.; Laghari, G.F.; Mansor, N.N. Fitness Dependent Optimizer-Based Automatic Generation Control of Multi-Source Interconnected Power System with Non-Linearities. *IEEE Access* **2020**, *8*, 100989–101003. [CrossRef]
26. Raj, U.; Shankar, R. Deregulated Automatic Generation Control using Novel Opposition-based Interactive Search Algorithm Cascade Controller Including Distributed Generation and Electric Vehicle. *Iran. J. Sci. Technol. Trans. Electr. Eng.* **2020**, *44*, 1233–1251. [CrossRef]
27. Kose, E. Optimal Control of AVR System with Tree Seed Algorithm-Based PID Controller. *IEEE Access* **2020**, *8*, 89457–89467. [CrossRef]
28. Kalyan, C.N.S.; Goud, B.S.; Reddy, C.R.; Ramadan, H.S.; Bajaj, M.; Ali, Z.M. Water Cycle Algorithm Optimized Type II Fuzzy Controller for Load Frequency Control of a Multi-Area, Multi-Fuel System with Communication Time Delays. *Energies* **2021**, *14*, 5387. [CrossRef]
29. Tripathy, S.; Debnath, M.K.; Kar, S.K. Optimal Design of Fractional Order 2DOF-PID Controller for Frequency Control in Interconnected System. In *Green Technology for Smart City and Society*; Springer: Singapore, 2020; pp. 23–33. [CrossRef]
30. Sahu, P.C.; Prusty, R.C.; Sahoo, B.K. Modified sine cosine algorithm-based fuzzy-aided PID controller for automatic generation control of multiarea power systems. *Soft Comput.* **2020**, *24*, 12919–12936. [CrossRef]
31. Ajithapriyadarsini, S.; Mary, P.M.; Iruthayarajan, M.W. Automatic generation control of a multi-area power system with renewable energy source under deregulated environment: Adaptive fuzzy logic-based differential evolution (DE) algorithm. *Soft Comput.* **2019**, *23*, 12087–12101. [CrossRef]
32. Çelik, E. Design of new fractional order PI–fractional order PD cascade controller through dragonfly search algorithm for advanced load frequency control of power systems. *Soft Comput.* **2020**, *25*, 1193–1217. [CrossRef]
33. Daraz, A.; Malik, S.A.; Mokhlis, H.; Haq, I.U.; Zafar, F.; Mansor, N.N. Improved-Fitness Dependent Optimizer Based FOI-PD Controller for Automatic Generation Control of Multi-Source Interconnected Power System in Deregulated Environment. *IEEE Access* **2020**, *8*, 197757–197775. [CrossRef]
34. Daraz, A.; Malik, S.A.; Haq, I.U.; Khan, K.B.; Laghari, G.F.; Zafar, F. Modified PID controller for automatic generation control of multi-source interconnected power system using fitness dependent optimizer algorithm. *PLoS ONE* **2020**, *15*, e0242428. [CrossRef] [PubMed]
35. Biswas, S.; Roy, P.K.; Chatterjee, K. FACTS-based 3DOF-PID Controller for LFC of Renewable Power System Under Deregulation Using GOA. *IETE J. Res.* **2021**, 1–14. [CrossRef]
36. Fathy, A.; Kassem, A.M.; Abdelaziz, A.Y. Optimal design of fuzzy PID controller for deregulated LFC of multi-area power system via mine blast algorithm. *Neural Comput. Appl.* **2018**, *32*, 4531–4551. [CrossRef]
37. Daraz, A.; Malik, S.A.; Azar, A.T.; Aslam, S.; Alkhalifah, T.; Alturise, F. Optimized Fractional Order Integral-Tilt Derivative Controller for Frequency Regulation of Interconnected Diverse Renewable Energy Resources. *IEEE Access* **2022**, *10*, 43514–43527. [CrossRef]
38. Zhao, S.; Zhang, T.; Ma, S.; Chen, M. Dandelion Optimizer: A nature-inspired metaheuristic algorithm for engineering applications. *Eng. Appl. Artif. Intell.* **2022**, *114*. [CrossRef]
39. Alsattar, H.A.; Zaidan, A.A.; Zaidan, B.B. Novel meta-heuristic bald eagle search optimisation algorithm. *Artif. Intell. Rev.* **2019**, *53*, 2237–2264. [CrossRef]
40. Qais, M.H.; Hasanien, H.M.; Alghuwainem, S. Transient search optimization: A new meta-heuristic optimization algorithm. *Appl. Intell.* **2020**, *50*, 3926–3941. [CrossRef]
41. Rahman, C.M.; Rashid, T.A. A new evolutionary algorithm: Learner performance based behavior algorithm. *Egypt. Inform. J.* **2020**, *22*, 213–223. [CrossRef]
42. Fathy, A.; Alharbi, A.G.; Alshammari, S.; Hasanien, H.M. Archimedes optimization algorithm based maximum power point tracker for wind energy generation system. *Ain Shams Eng. J.* **2021**, *13*, 101548. [CrossRef]
43. Zou, H.; Li, H. Tuning of PI–PD controller using extended non-minimal state space model predictive control for the stabilized gasoline vapor pressure in a stabilized tower. *Chemom. Intell. Lab. Syst.* **2015**, *142*, 1–8. [CrossRef]

44. Raja, G.L.; Ali, A. New PI-PD Controller Design Strategy for Industrial Unstable and Integrating Processes with Dead Time and Inverse Response. *J. Control. Autom. Electr. Syst.* **2021**, *32*, 266–280. [CrossRef]
45. Kaya, I. Optimal PI–PD Controller Design for Pure Integrating Processes with Time Delay. *J. Control. Autom. Electr. Syst.* **2021**, *32*, 563–572. [CrossRef]
46. Irshad, M.; Ali, A. Robust PI-PD controller design for integrating and unstable processes. *IFAC-PapersOnLine* **2020**, *53*, 135–140. [CrossRef]
47. Peram, M.; Mishra, S.; Vemulapaty, M.; Verma, B.; Padhy, P.K. Optimal PI-PD and I-PD Controller Design Using Cuckoo Search Algorithm. In Proceedings of the 5th International Conference on Signal Processing and Integrated Networks, Delhi, India, 22–23 February 2018; pp. 643–646. [CrossRef]
48. Deniz, F.N.; Yüce, A.; Tan, N. Tuning of PI-PD Controller Based on Standard Forms for Fractional Order Systems. *J. Appl. Nonlinear Dyn.* **2018**, *8*, 5–23. [CrossRef]
49. Zheng, M.; Huang, T.; Zhang, G. A New Design Method for PI-PD Control of Unstable Fractional-Order System with Time Delay. *Complexity* **2019**, *2019*, 1–12. [CrossRef]
50. Ali, T.; Adeel, M.; Malik, S.A.; Amir, M. Stability Control of Ball and Beam System Using Heuristic Computation Based PI-D and PI-PD Controller. *Tech. J. Univ. Eng. Technol.* **2019**, *24*, 21–29.
51. Tian, D.; Shi, Z. MPSO: Modified particle swarm optimization and its applications. *Swarm Evol. Comput.* **2018**, *41*, 49–68. [CrossRef]